Early solar irradiation as a source of the inner solar system chromium isotopic heterogeneity

Yogita KADLAG [1,2]*, Jason HIRTZ[2], Harry BECKER[1], Ingo LEYA [2], and Klaus MEZGER[3]

[1]Institut für Geologische Wissenschaften, Freie Universität Berlin, Malteserstr. 74-100, Berlin 12249, Germany
[2]Physikalisches Institut, Universität Bern, Sidlerstrasse 5, Bern 3012, Switzerland
[3]Institut für Geologie, Universität Bern, Baltzerstrasse 1+3, Bern 3012, Switzerland
*Corresponding author. Email: yogita.kadlag@space.unibe.ch

Abstract–Different solar system objects display variable abundances of neutron-rich isotopes such as ^{54}Cr, ^{50}Ti, and ^{48}Ca, which are commonly attributed to a heterogeneous distribution of presolar grains in different domains of the solar system. Here, we show that the heterogeneity of ^{54}Cr/^{52}Cr and the correlation of ^{54}Cr/^{52}Cr with Fe/Cr in metal fractions of EH3 chondrites and in inner solar system bodies can be attributed to variable irradiation of dust grains by solar energetic particles and variable mixing of irradiated material in the different domains of the inner solar nebula. The isotope variations in inner solar system objects can be generated by ~300 y long local irradiation of mm- to cm-sized solids with average solar energetic particle fluxes of ~10^5 times the modern value. The relative homogeneity of ^{53}Cr/^{52}Cr in inner solar system objects can be a consequence of the production of ^{53}Mn by the early irradiation of dust, evaporation, and nebula-wide homogenization of Mn due to high temperatures, followed by Mn/Cr fractionation within the first few million years of the solar system. The ^{54}Cr/^{52}Cr of the Earth can be produced by irradiated pebbles and <15 wt% of CI chondrite like material. Alternatively, Earth may contain only a few % of CI chondrite like material but then must have an Fe/Cr ratio 10–15% higher than CI chondrites.

INTRODUCTION

The solar system shows large-scale heterogeneity in the abundances of the neutron-rich isotopes near the iron peak, such as ^{54}Cr, ^{50}Ti, and ^{48}Ca, with systematic differences between inner and outer solar system bodies (e.g., Schiller et al., 2018; Trinquier et al., 2007, 2009; Warren, 2011). These variations have been attributed to variable contributions from presolar grains that record extreme isotopic compositions, because they formed in different stellar environments (e.g., Hartmann et al., 1985; Nittler et al., 2018; Trinquier et al., 2007; Wasserburg et al., 2015; Woosley, 1997). The distinct ε^{54}Cr ranges (ε-values represent parts in 10,000 abundance variations of ^{54}Cr) in noncarbonaceous meteorites (NC) and in the carbonaceous chondrites and related meteorite groups (CC) are currently explained by the early separation of two distinct reservoirs in the solar nebula. NC meteorites comprise objects from the inner solar system, whereas CC meteorites are interpreted to comprise objects from beyond Jupiter, that

is, at greater heliocentric distances than NC meteorites (Boss, 2004; Kruijer et al., 2017; Warren, 2011). In contrast, variations of ^{53}Cr in meteorites are mainly explained by variable abundances of the short-lived ^{53}Mn that decays to ^{53}Cr (e.g., Lugmair & Shukolyukov, 1998; Trinquier et al., 2008).

Bulk CC meteorites display correlated variations of ε^{54}Cr with ε^{53}Cr (Qin et al., 2010; Shukolyukov & Lugmair, 2006; Trinquier et al., 2008). This was explained by the addition of ^{54}Cr and ^{53}Cr from supernova remnants into the nascent solar nebula (Boss, 2004; Hartmann et al., 1985; Woosley, 1997). However, there is also a correlation of Cr isotopes in bulk CC with Mn/Cr, which suggests a link with chemical variation resulting from thermal processing of dust (Göpel et al., 2015; Qin, et al., 2010; Shukolyukov & Lugmair, 2006; Trinquier et al., 2008). Dauphas et al. (2010), Nittler et al. (2018), and Qin et al. (2011) reported strongly ^{54}Cr-enriched oxide nanoparticles extracted from carbonaceous chondrites. In contrast, NC meteorites (enstatite [EC] and ordinary chondrites [OC]

and meteorites from differentiated parent bodies such as ureilites, angrites, and HED [howardite–eucrite–diogenite] meteorites), bulk silicate Earth, and meteorites from Mars show no correlation of $\varepsilon^{54}Cr$ with $\varepsilon^{53}Cr$ and all have lower $\varepsilon^{54}Cr$ compared to CC (Trinquier et al., 2009; Warren, 2011). Furthermore, NC meteorites show up to 1ε unit heterogeneity in $\varepsilon^{54}Cr$; however, the control of bulk ^{54}Cr variations in NC chondrites by carriers with extreme enrichments of ^{54}Cr is unclear (Trinquier et al., 2009; Warren, 2011). The variations of $\varepsilon^{54}Cr$ among inner and outer solar system bodies were interpreted to reflect incomplete mixing of presolar dust from supernovae across the protoplanetary disk (Boss, 2004; Olsen et al., 2016; Trinquier et al., 2007). Possible causes for the $\varepsilon^{54}Cr$ heterogeneity include the gravitational force of rapidly growing planetary embryos, a growing Jupiter (Kruijer et al., 2017), or the selective destruction of ^{54}Cr carriers by thermal processing (e.g., chondrule formation events) in the inner solar system (Sugiura & Fujiya, 2014; Trinquier et al., 2007). However, if the flux of freshly injected supernova material was directed from the outer to the inner solar system and was partially blocked by proto-Jupiter, then $\varepsilon^{54}Cr$ within the inner solar system should decrease toward the Sun, which does not appear to be the case (Trinquier et al., 2009). Also, thermal destruction of ^{54}Cr carriers should have occurred more efficiently in objects closer to the Sun (e.g., Earth and ECs) compared to objects far away from the Sun (e.g., OC, Mars, Vesta, ureilite parent body [UPB]). Yet, the data show the opposite; ECs, which presumably formed closer to the Sun than other meteorites, have higher $\varepsilon^{54}Cr$ than OC and HED meteorites (Qin et al., 2010; Trinquier et al., 2007). The differences in ^{54}Cr (Trinquier et al., 2007, 2009) and other neutron-rich isotopes among solar system bodies and the presumed addition of variable amounts of supernova material are difficult to reconcile with evidence for homogeneous initial $\varepsilon^{53}Cr$ and ^{26}Al in inner solar system bodies, and the proposed homogeneous distribution of ^{53}Mn in the solar system (Trinquier et al., 2008; Villeneuve et al., 2009). Thus, the chronology and nature of the processes that led to these observations are yet to be understood.

The highly reduced mineralogy and the oxygen isotope composition of enstatite chondrites suggest their origin in the innermost region of the solar system, that is, at a heliocentric distance of <1 AU (Clayton et al., 1984; Larimer & Bartholomay, 1979; Mason, 1966). Trace mineral carriers of ^{54}Cr that were identified in carbonaceous chondrites, such as Cr-rich spinels (Dauphas et al., 2010; Qin et al., 2011; Nittler et al., 2018), have not been reported in enstatite chondrites, presumably because of the strongly reducing conditions under which enstatite chondrites formed, which would lead to destruction of Cr spinel and partitioning of Cr

into sulfides. Therefore, the study of the origin of the variation of mass-independent Cr isotope composition could benefit from analysis of mechanically separated components of unequilibrated ECs, in combination with data on chemical leachates.

This study provides new Cr isotope data on components of EH3 chondrites such as chondrules, metal troilite spherules (MTS), matrix metal, and silicates together with data on leachates. The new data are compared with literature Cr isotope data and Fe/Cr variations of inner solar system objects to investigate whether early solar energetic particle irradiation could be an alternative process that might have produced enrichments in the neutron-rich isotopes ^{53}Cr and ^{54}Cr. The goal is to constrain nebular conditions, possible time scales, and solar energetic particle fluxes that may have affected Cr isotope compositions of inner solar system objects.

MATERIALS AND METHODS

Mechanically separated components from the two EH3 enstatite chondrites Kota Kota and Sahara 97072 were studied. BHVO-2, UBN, and Allende standard reference powders were also analyzed as reference materials to verify the validity of the analytical method used for Cr isotope measurements.

Approximately 1 g chips of each Kota Kota and Sahara 97072 were broken into pieces. Components such as chondrules, irregular shaped white aggregates (mostly SiO_2 with intergrown enstatite and other minerals), and MTSs were separated manually from the broken pieces. The remaining material was gently crushed in an agate mortar and separated into different size fractions (<80, 80–150, 150–200, 200–250, and >250 μm) using nylon sieves, followed by separation into magnetic, slightly magnetic, and nonmagnetic fractions. Magnetic fractions mainly contain Fe-Ni metal with some associated sulfides, whereas the slightly magnetic fractions are dominated by sulfides and silicates. Mechanically and magnetically separated samples were dissolved in reverse aqua regia in a high-pressure asher at 320 °C. A fraction of the sample solution was analyzed for concentrations of highly siderophile elements, S-Se-Te, and major elements (Kadlag & Becker, 2015).

About 60 mg of bulk rock powder of Kota Kota was used for the leaching procedure and subsequent chemical separation of Cr. The procedure for the chemical dissolution of the whole rock powder of Kota Kota (procedure from Petitat et al., 2011) is summarized in Table 1. After each step, the supernatant was collected in a separate beaker, dried down at 80 °C, and converted into chloride form before separation of Cr from matrix

Table 1. Chemical dissolution procedure for Kota Kota whole rock powder.

Leaching step	Acid	Parameters (time, temperature)
L1	0.4 N CH$_3$COOH	30 minutes, 25 °C
L2	8.5 N CH$_3$COOH	1 day, 25 °C
L3	0.5 N HNO$_3$	1 day, 25 °C
L4	4 N HNO$_3$	7 days, 25 °C
L5	14 N HNO$_3$ + 27 N HF	4 days, 100 °C
L6	14 N HNO$_3$ + 27 N HF	10 days, 150 °C

elements by a two-step ion exchange column chromatography procedure. Iron was removed using 2 mL Eichrom anion exchange resin (1-X8, 100–200 mesh) and 6 M HCl. The Cr cut from the first separation step was dried down and dissolved in 1.5 M HCl. The second separation step was carried out on glass columns using 2.4 mL Bio-Rad cation exchange resin (AG50-X12 200–400) to remove Al, Ti, Na, Mg, V, and Mn. The recovery of Cr in the first separation step was >99% for most samples, and in the second separation step, it was >95% for all samples. Blank contributions (<1 ng) are negligible compared to the total amount of Cr in the sample aliquots. The Cr separation procedure is described in Kadlag et al. (2019).

Chromium isotope ratios were measured as positive ions on a ThermoFinnigan Triton thermal ionization mass spectrometer at Freie Universität Berlin. A mixture of purified Cr in chloride form, H$_3$BO$_3$, and silica gel was loaded on single Re filaments. The filaments were heated to 2100–2300 mA and isotope ratio measurements (28 blocks × 20 cycles for each measurement) were carried out once a stable signal of 4–10 V for ^{52}Cr was achieved. The baseline was measured after seven blocks (30 cycles, counting time = 1.05 s/cycle, and pre-baseline wait time = 10 s), and amplifier rotation was applied after every seventh block to eliminate cup biases. The ^{54}Fe can be a significant interfering mass on ^{54}Cr during analysis. Therefore, two independent tests were carried out to check for Fe in the samples. Anion column separation may not remove all Fe from Cr. Therefore, after every separation (for each sample), the Fe concentration in the Cr separate was routinely checked by inductively coupled plasma mass spectrometry (ICP-MS). For all cases, the Fe concentration in the Cr cut was similar to the blank contribution and thus negligible. In addition, we always monitored the Fe signal by thermal ionization mass spectrometry (TIMS). ^{56}Fe is measured simultaneously with Cr isotopes and a correction is applied on ^{54}Cr during data reduction. For all samples, ^{56}Fe signals were low and ^{56}Fe/^{52}Cr ratio was always

<0.0001 (average = 0.00001). Therefore, the contribution from ^{54}Fe on ^{54}Cr is negligible.

The Cr isotopic compositions of samples are reported relative to the NIST SRM 3112a (Lot No.030730) Cr reference material as ε^iCr,

$$\varepsilon^i\text{Cr} = \left[\frac{\left(\frac{i_{\text{Cr}}}{52_{\text{Cr}}}\right)_{\text{Sample}}}{\left(\frac{i_{\text{Cr}}}{52_{\text{Cr}}}\right)_{\text{NIST 3112a}}} - 1 \right] \times 10^4 \qquad (1)$$

where i = 53 or 54.

Two to three micrograms of sample Cr were loaded on one to three filaments (depending on the available amount of Cr) and each filament was measured twice. For each measurement session (two analyses on a single filament), repeatability of Cr isotope measurements for the Cr standard NIST 3112a was better than ±0.10ε (2σ) for ε^{53}Cr and better than ±0.20ε for ε^{54}Cr. Long-term precision for the NIST 3112a standard over the period of measurements is 0.06ε for ε^{53}Cr and 0.13ε for ε^{54}Cr (Table S1 in supporting information). The reference materials UB-N (serpentinite powder, Col de Bagenelles France; Govindaraju, 1982), BHVO-2 (Hawaiian basalt; Wilson, 1997), and the Allende meteorite powder (Smithsonian standard powder, USNM 3529, Split 18 position 1) were also analyzed using the same procedure.

Mn/Cr and Fe/Cr ratios of dilutions of the sample solutions were analyzed in medium resolution mode on an Element XR$^{\text{TM}}$ ICP-MS at Freie Universität Berlin. Calibrations were performed using dilutions of a gravimetrically prepared Mn-Cr standard solution and BHVO-2 reference material. Instrumental drift was corrected by analysis of standard solutions.

RESULTS

The determined Cr isotope compositions; Mn/Cr and Fe/Cr ratios of mechanically and magnetically separated components of the unequilibrated enstatite chondrites Kota Kota (EH3) and Sahara 97072 (EH3); the differentially dissolved mineral phases of Kota Kota; and the reference materials UBN, BHVO-2, and Allende are presented in Table 2 and are discussed in following sections.

Reference Materials

The ε^{53}Cr and ε^{54}Cr values of the reference materials UB-N, BHVO-2, and Allende are 0.00 ± 0.08, 0.01 ± 0.08, and 0.05 ± 0.08 and 0.05 ± 0.14, 0.05 ± 0.14, and 0.85 ± 0.14, respectively (Table 2). The ^{55}Mn/^{52}Cr ratio of the reference materials UBN,

Table 2. Ratios of Fe/Cr, Mn/Cr, and Cr isotopes in physically separated components of Sahara 97972 and Kota Kota; differentially dissolved mineral phases of Kota Kota; and reference materials.

Sample name	Chemical composition	n	Fe/Cr $\pm$ 2SD	$^{55}Mn/^{52}Cr$ $\pm$ 2SD	$\varepsilon^{53}Cr \pm 2SE$	$\varepsilon^{54}Cr \pm 2SE$
Sahara 97072						
Sah-SM (<80 μm)	16 Me + 9 S + 75 Si	4	58 ± 6	0.69 ± 0.04	0.26 ± 0.09	0.29 ± 0.09
Sah-SM (80–150 μm)	19 Me + 7 S + 73 Si	1	60 ± 8	0.65 ± 0.06	0.17 ± 0.09	0.02 ± 0.21
Sah-SM (150–200 μm)	19 Me + 9 S + 72 Si	3	89 ± 7	0.79 ± 0.05	0.26 ± 0.08	0.26 ± 0.12
Sah-SM (200–250 μm)	17 Me + 8 S + 75 Si	2	97 ± 6	1.24 ± 0.08	0.19 ± 0.07	0.24 ± 0.17
Sah-SM (> 250 μm)	21 Me + 6 S + 73 Si	5	72 ± 8	0.54 ± 0.05	0.01 ± 0.09	0.11 ± 0.09
Sah-M (80–150 μm)	47 Me + 13 S + 40 Si	4	139 ± 5	0.81 ± 0.14	0.25 ± 0.04	0.36 ± 0.15
Sah-M (200–250 μm)	32 Me + 14 S + 54 Si	3	110 ± 4	0.75 ± 0.06	0.19 ± 0.09	0.12 ± 0.18
Sah-M (> 250 μm)	28 Me + 12 S + 60 Si	1	92 ± 8	0.82 ± 0.06	0.25 ± 0.11	0.26 ± 0.25
Sah-MTS	30 Me + 13 S + 57 Si	4	245 ± 15	1.33 ± 0.09	−0.02 ± 0.11	−0.46 ± 0.29
Sah-WMP	5 Me + 3 S + 92 Si	3	27 ± 2	0.67 ± 0.05	0.20 ± 0.09	0.53 ± 0.20
Sah-NM	3 Me + 5 S + 92 Si	2	17 ± 1	0.67 ± 0.10	0.15 ± 0.04	0.01 ± 0.07
Sah-bulk magnetic	Me + S	6	133 ± 14	0.73 ± 0.03	0.24 ± 0.05	0.35 ± 0.12
Kota Kota						
KK-SM (<80 μm)	6 Me + 15 S + 79 Si	4	42 ± 3	0.79 ± 0.07	0.25 ± 0.07	0.20 ± 0.17
KK-SM (80–150 μm)	8 Me + 12 S + 80 Si	2	47 ± 4	0.81 ± 0.07	0.31 ± 0.04	0.25 ± 0.17
KK-SM (150–200 μm)	11 Me + 11 S + 78 Si	4	57 ± 6	0.91 ± 0.10	0.15 ± 0.05	0.07 ± 0.16
KK-SM (200–250 μm)	5 Me + 9 S + 86 Si	4	40 ± 5	0.98 ± 0.12	0.23 ± 0.04	0.21 ± 0.17
KK-SM (>250)	8 Me + 8 S + 84 Si	4	42 ± 7	0.75 ± 0.06	0.10 ± 0.05	−0.02 ± 0.17
KK-M (<80 μm)	38 Me + 12 S + 50 Si	4	135 ± 8	0.78 ± 0.04	0.39 ± 0.08	0.43 ± 0.09
KK-M (80–150 μm)	41 Me + 12 S + 47 Si	2	141 ± 6	0.71 ± 0.07	0.35 ± 0.08	0.59 ± 0.12
KK-M (150–200 μm)	41 Me + 13 S + 47 Si	4	136 ± 6	0.73 ± 0.06	0.28 ± 0.05	0.25 ± 0.19
KK-M (200–250 μm)	41 Me + 13 S + 46 Si	2	137 ± 5	0.71 ± 0.09	0.29 ± 0.09	0.33 ± 0.12
KK-WMP	20 Me + 9 S + 71 Si	1	69 ± 7	0.62 ± 0.05	0.13 ± 0.08	0.19 ± 0.17
KK-chondrules	7 Me + 8 S + 84 Si	2	40 ± 1	0.82 ± 0.03	−0.06 ± 0.07	−0.20 ± 0.15
KK-bulk magnetic	Me + S	8	n.d.	0.73 ± 0.10	0.39 ± 0.03	0.60 ± 0.10
Kota Kota leachate						
L1	Me + S	1	726 ± 23	22.0 5 ± 0.90	1.33 ± 0.08	−0.04 ± 0.22
L2	Me + S	3	612 ± 19	2.84 ± 0.12	0.68 ± 0.10	0.56 ± 0.14
L3	Me + S	2	325 ± 10	0.28 ± 0.01	0.27 ± 0.08	0.54 ± 0.14
L4	Me + S + Si	3	9.6 ± 0.3	0.050 ± 0.002	0.29 ± 0.08	0.62 ± 0.26
L5	Si	4	13.3 ± 0.4	0.66 ± 0.03	0.02 ± 0.08	−0.15 ± 0.14
L6	Si	2	65 ± 2	0.19 ± 0.01	0.03 ± 0.11	0.00 ± 0.14
Reference materials						
UBN		4	26 ± 3	0.45 ± 0.04	0.00 ± 0.08	0.05 ± 0.14
BHVO-2		3	304 ± 21	4.54 ± 0.17	0.01 ± 0.08	0.05 ± 0.14
Allende		5	67 ± 2	0.50 ± 0.03	0.05 ± 0.08	0.85 ± 0.14

x Me + y S + z Si = x wt% metal + y wt% sulfides + z wt% silicates.

n = number of Cr isotopic analyses; n.d. = no data; M = magnetic; Me = metal; S = sulfides; Si = Ssilicates; SM = slightly magnetic; N = nonmagnetic; WMP = white mineral phases.

BHVO-2, and Allende are 0.45 ± 0.04, 4.54 ± 0.17, 0.50 ± 0.03 (Table 2). The $\varepsilon^{53}Cr$ and $\varepsilon^{54}Cr$ values of the reference materials are consistent with literature data (Qin et al., 2010; Trinquier et al., 2008), which confirms the validity of the method at the given level of precision.

Physically Separated Components

The results for $\varepsilon^{53}Cr$ and $\varepsilon^{54}Cr$ together with the $^{55}Mn/^{52}Cr$ ratio in the mechanically separated components of Sahara 97072 and Kota Kota are given in Table 2. The total variation of ^{54}Cr in the physically separated components of EH3 chondrites is 1.05ε.

Magnetic, slightly magnetic, and chondrule fractions show a correlation between $\varepsilon^{53}Cr$ and $\varepsilon^{54}Cr$, however, with different slopes (Fig. 1; Figs. S1 and S2). The slopes of the $\varepsilon^{53}Cr$-$\varepsilon^{54}Cr$ correlation of metal-rich fractions of Kota Kota and Sahara 97072 are 3.3 ± 0.7 and 3.9 ± 0.1, respectively. Excluded from this correlation are Sah-M (>250 μm) and the MTS fraction due to their high abundances of silicates and sulfides.
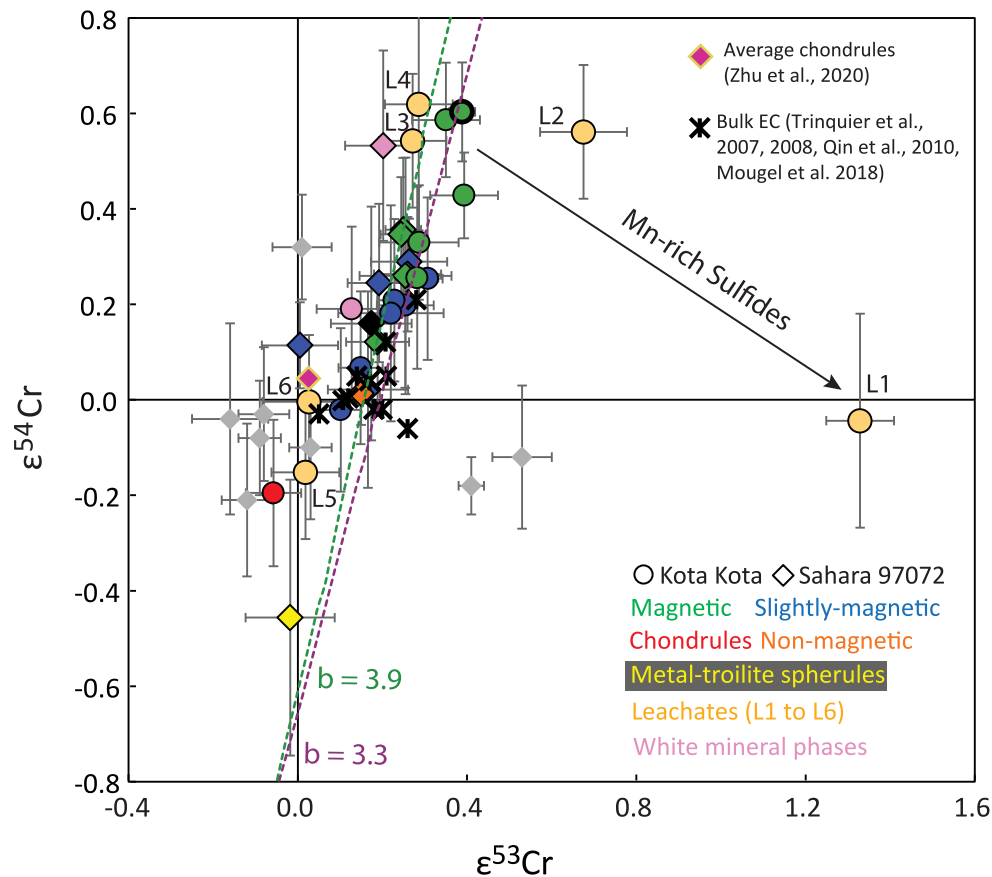
Fig. 1. ε^{54}Cr versus ε^{53}Cr in physically separated components of the EH3 chondrites Kota Kota and Sahara 97072 together with data for chemical leachates of Kota Kota. The gray symbols are literature data for individual chondrule (Zhu et al., 2019, 2020) of Sahara 97096 (paired to Sahara 97072). Black crosses are literature data for whole rock samples from enstatite chondrites (Qin et al., 2010; Trinquier et al., 2007, 2008). Specific components define correlation lines with different slopes (See Fig. S2 for details). The slopes (b) of metal-rich, magnetic fractions from Kota Kota (b = 3.3 ± 0.7) and Sahara 97072 (b = 3.9 ± 0.1) are highlighted. Galactic cosmic ray (GCR) induced contributions to ^{54}Cr and ^{53}Cr calculated using the known exposure ages for both meteorites are negligible. (Color figure can be viewed at wileyonlinelibrary.com.)

Corrections of the Cr isotope data for the effects of cosmic ray-induced spallation using their measured Fe/Cr ratios and exposure ages of 20–30 Myr (Patzer & Schultz, 2001) are insignificant (Fig. S1).

Differentially Dissolved Phases of Kota Kota

In differentially dissolved phases (here called "leachates") of Kota Kota, Fe/Cr ratios range from 10 (leachate L4) to 726 (leachate L1). The ^{55}Mn/^{52}Cr ratios in leachates range from 0.19 ± 0.01 to 22.0 ± 0.9 (Table 2); ε^{53}Cr and ε^{54}Cr in the leachates of Kota Kota range from 0.02 ± 0.08 to 1.33 ± 0.08 and −0.15 ± 0.14 to 0.62 ± 0.26, respectively. The absolute variation of ^{54}Cr in the leachates is 0.77ε (Fig. 1). Leachates from Kota Kota display enrichments of ^{53}Cr, most prominently in the Mn-rich leachates that include dissolved sulfides (L1 and L2; see Fig. 3a). Overall, the

leachates either show correlated ^{53}Cr and ^{54}Cr or radiogenic ^{53}Cr that varies independently of ^{54}Cr.

DISCUSSION

Relationships Between ^{54}Cr, ^{53}Cr, and the Composition of Enstatite Chondrite Components

The new ε^{53}Cr and ε^{54}Cr data on components of EH3 chondrites yield two key results (see also Table 2; Fig. 2). First, Fe-Ni metal-rich magnetic fractions of Kota Kota and Sahara 97072 display linear correlations between spallation-corrected ε^{53}Cr and ε^{54}Cr with slopes of ~3.3 ± 0.7 and 3.9 ± 0.1, respectively (Fig. 1; Fig. S1). Second, ^{54}Cr-enriched magnetic fractions have high Fe/Cr and magnetic fractions with lower ε^{54}Cr have lower Fe/Cr ratios and that magnetic fractions tend to have higher ε^{54}Cr than nonmagnetic or less

magnetic fractions. These relationships indicate that the process that led to the ^{54}Cr enrichment in these enstatite chondrites is related to the chemical composition, and more specifically to the Fe content of the material. ε^{54}Cr values in magnetic fractions (excluding Sah-M [>250 μm] fraction, because of its high sulfide and silicate content and low Fe-Ni metal content) show a linear correlation with Fe/Cr (Fig. 2) yielding ε^{54}Cr of −1.1 ± 0.5 at Fe/Cr = 0. The intercept agrees within uncertainty with the intercept of ε^{54}Cr = −1.5 at Fe/Cr = 0 defined by ε^{54}Cr-Fe/Cr variations of inner solar system bodies (Fig. 2).

The data obtained from the different meteorite components suggests that the ε^{54}Cr values of bulk enstatite chondrites represent the mixtures of ^{54}Cr-rich metal with ^{54}Cr-poor sulfides and silicates (Fig. S3). Furthermore, matrix metal and metal from separated metal–troilite spherules show different ε^{54}Cr (Fig. 2). The differences in ε^{54}Cr between matrix metal, MTS, metal, and sulfide–silicate-rich fractions must result from pre-accretionary processes and they are also evidence for the unequilibrated nature of EH3 chondrites.

^{53}Mn-^{53}Cr Systematics of Physically Separated Components and Leachates

Chromium in enstatite chondrites is mainly hosted in sulfides like daubréelite (Ramdohr, 1963) and troilite (Weyrauch et al., 2018; Zhang et al., 1995). In other sulfides as well as in silicates and metal, it can be a minor or trace element (Kadlag et al., 2019; Mason, 1966). MTSs from Sahara 97072 have lower ε^{53}Cr and ε^{54}Cr compared to all other fractions (Fig. 1). ε^{53}Cr and ^{55}Mn/^{52}Cr in the separated components of Kota Kota and Sahara 97072 scatter around the bulk rock value (Fig. 3). Higher ε^{53}Cr in magnetic fractions do not correlate with higher ^{55}Mn/^{52}Cr. This scatter likely results from diffusive redistribution of Mn or Cr on the meteorite parent body following decay of ^{53}Mn (Fig. 3). An internal ^{53}Mn-^{53}Cr errorchron of the leachates from Kota Kota yields an apparent age of 4555 ± 2 Ma (Fig. 3a), assuming solar system initial ^{53}Mn/^{55}Mn = (6.28 ± 0.66) x 10^{-6} at 4567.3 Ma (Trinquier et al., 2008). The slope of the errorchron is controlled by leachate L1 (Fig. 3b), which is dominated by Mn-rich sulfides. The young age suggests late modification (>9 Myr after calcium–aluminum-rich inclusion [CAI] formation at 4567.3 Ma) of the Mn-Cr system on the parent body of EH3 chondrites. A lower ^{53}Mn/^{55}Mn than the solar system initial was also reported previously for a sulfide grain (sphalerite, ZnS) from Kota Kota (Wadhwa et al., 1997) and was attributed to diffusive redistribution of Cr on the parent body.

Origin of ^{54}Cr Variations in EH3 Chondrites: Evaluation of the Hypothesis of Different Presolar Components and the Role of Mixing

Previous studies suggested variable mixing of presolar grains and destruction of some of these grains at high temperatures as an explanation for the heterogeneous distribution of ^{54}Cr in the solar system (e.g., Qin et al., 2010; Trinquier et al., 2009; and references therein). In CCs, high ε^{54}Cr values occur in refractory inclusions and in minute Cr spinels enriched in ^{54}Cr, which are considered to be the carriers of the ^{54}Cr enrichment in the bulk CC meteorites relative to Earth and other chondrites (Dauphas et al., 2010; Nittler et al., 2018).

It is commonly assumed that the flux of freshly injected supernova material was directed from the outer to the inner solar system (e.g., Olsen et al., 2016). In such a case, ε^{54}Cr within the inner solar system should decrease toward the Sun. However, ECs, which are considered to have formed <1 AU (Clayton et al., 1984; Larimer & Bartholomay, 1979; Mason, 1966) have higher ε^{54}Cr than OCs and NC-type achondrite meteorites that are interpreted to derive from further out in the inner solar system (Qin et al., 2010; Trinquier et al., 2009). The limited variation of ε^{54}Cr in the EH3 leachates (0.74ε) and in physically separated components (1ε) may reflect the destruction of ^{54}Cr carriers and homogenization of pre-existing ε^{54}Cr anomalies during thermal processing. This may have occurred either in the solar nebula or on the meteorite parent body, albeit because of their unequilibrated nature and the possible ^{54}Cr carriers being refractory, equilibration on the parent body is difficult to conceive for EH3 chondrites. Refractory inclusions are very rare in ECs and thin sections of Kota Kota and Sahara 97072 prepared from material analyzed in the present study did not contain CAIs. EH chondrites also contain only little (if any) Al-Cr spinel, which rarely occurs as an igneous crystallization product in some chondrules (Birck & Allegre, 1988; Birck & Lugmair, 1988; Brearley & Jones, 1998; Fagan et al., 2000). However, because of the accessory nature of presolar grains, no correlation between ε^{53}Cr, ε^{54}Cr, and Fe/Cr is expected, because ^{53}Cr and ^{54}Cr are hosted in different carrier phases and redistribution of Cr isotopes should have occurred independently of the Fe/Cr ratio. If larger isotopic differences among components were destroyed during thermal processing, then refractory element-rich phases sampled by leachates L4, L5, and L6 should show larger ε^{54}Cr anomalies compared to leachates L1, L2, and L3 that accessed more labile phases. The correlation of ^{54}Cr with the Fe/Cr ratio suggests a dependence of the abundance of ^{54}Cr on the relative
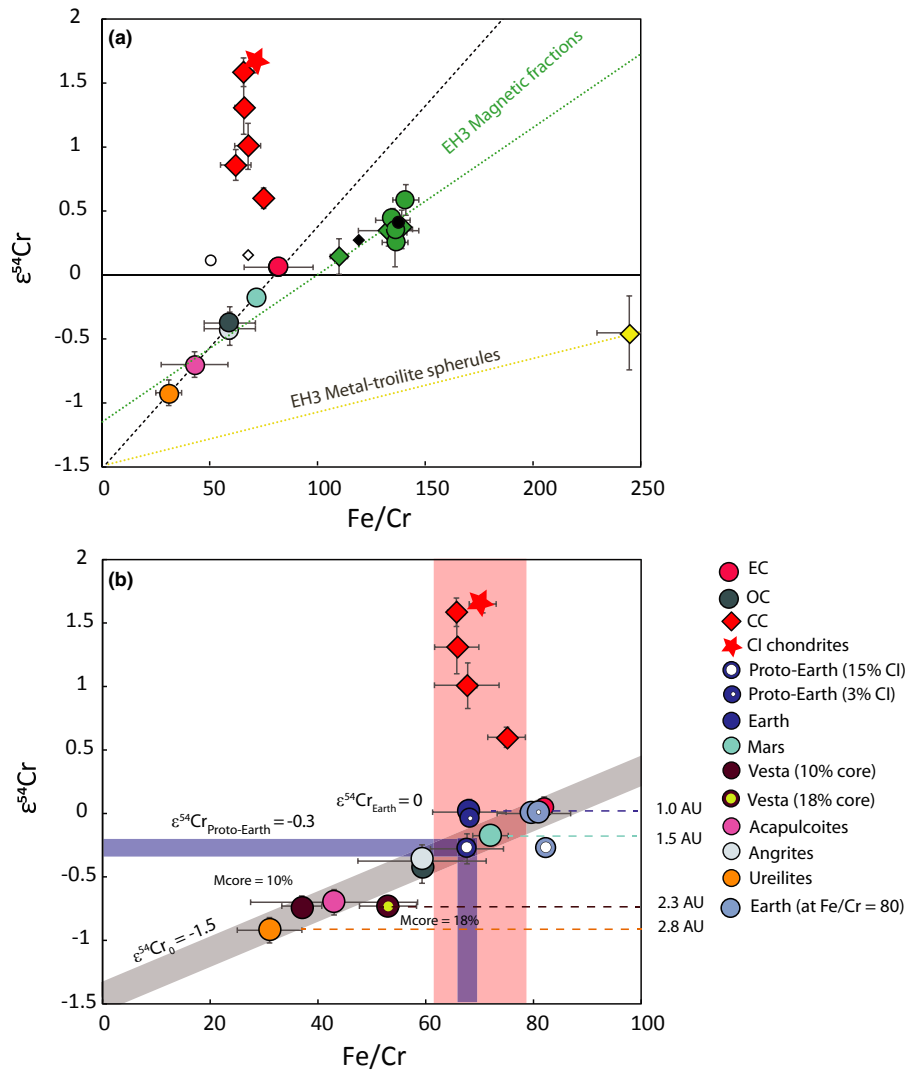
Fig. 2. a) ε^{54}Cr as a function of Fe/Cr in the metal-rich fractions of the unequilibrated EH3 chondrites Kota Kota and Sahara 97072 and in different solar system objects. The latter define an ε^{54}Cr$_{initial}$ (intercept at Fe/Cr = 0) of ~−1.5. The empty symbols are average values of non-magnetic and slightly magnetic fractions from Kota Kota and Sahara 97072; black symbols are average values for magnetic fractions. The correlation of inner solar system objects is defined by the mean values of ECs and OCs, Mars, acapulcoites, and ureilites. The compositions of bulk Vesta (the presumed HED meteorite parent body) and the angrite parent body are less well defined (see [b]) and supporting information. b) ε^{54}Cr versus Fe/Cr in solar system objects. The estimated bulk compositions of inner solar system objects define a linear correlation, with the notable exception of Earth. This correlation is interpreted to reflect early solar energetic particle (SEP) irradiation of the inner solar system as a function of heliocentric distance, with ECs and the Earth showing the strongest influence. The presumed proto-Earth represents the Earth before the Moon-forming giant impact and was obtained from the modern bulk silicate Earth, by subtraction of ~15% of a CI chondrite-like composition. Alternatively, Earth may have a Fe/Cr about 10–15% higher than CI chondrites and contains only a few % of a CI chondrite component. In this case, Earth falls on the inner solar system trend. For details see text and supporting information. The ε^{54}Cr and Fe/Cr values of CI chondrites (Lodders, 2003; Qin et al., 2010), CM chondrites (Göpel et al., 2015; Jarosewich, 1971; Kallemeyn & Wasson, 1981; Qin et al., 2010; Trinquier et al., 2007), CR (Trinquier et al., 2007, 2008; Weisberg et al., 1993), CV chondrites (Clarke et al., 1971; Kallemeyn & Wasson, 1981; Qin et al., 2010; Trinquier et al., 2007, 2008), CO (Göpel et al., 2015; Qin et al., 2010; Trinquier et al., 2007, 2008), OCs (Kallemeyn et al., 1989; Qin et al., 2010; Trinquier et al., 2007, 2008), ECs (Qin et al., 2010; Trinquier et al., 2007, 2008; Wasson & Kallemeyn, 1988; Weeks & Sears, 1985), UPB (Yamakawa et al., 2010), acapulcoites (Goodrich et al., 2017; Zipfel & Palme, 1994), angrites (Weiss et al., 2008; Zhu, Moynier, et al., 2019), Vesta (Dreibus & Wänke, 1980; Dreibus et al., 1997; Qin et al., 2010; Trinquier et al., 2007, 2008), Mars (Lodders & Fegley, 1997; Qin et al., 2010; Sanloup et al., 1999; Taylor, 2013; Trinquier et al., 2007; Wänke & Dreibus, 1994), Earth (McDonough, 2003; Trinquier et al., 2007, 2008) are from different literature sources. (Color figure can be viewed at wileyonlinelibrary.com.)
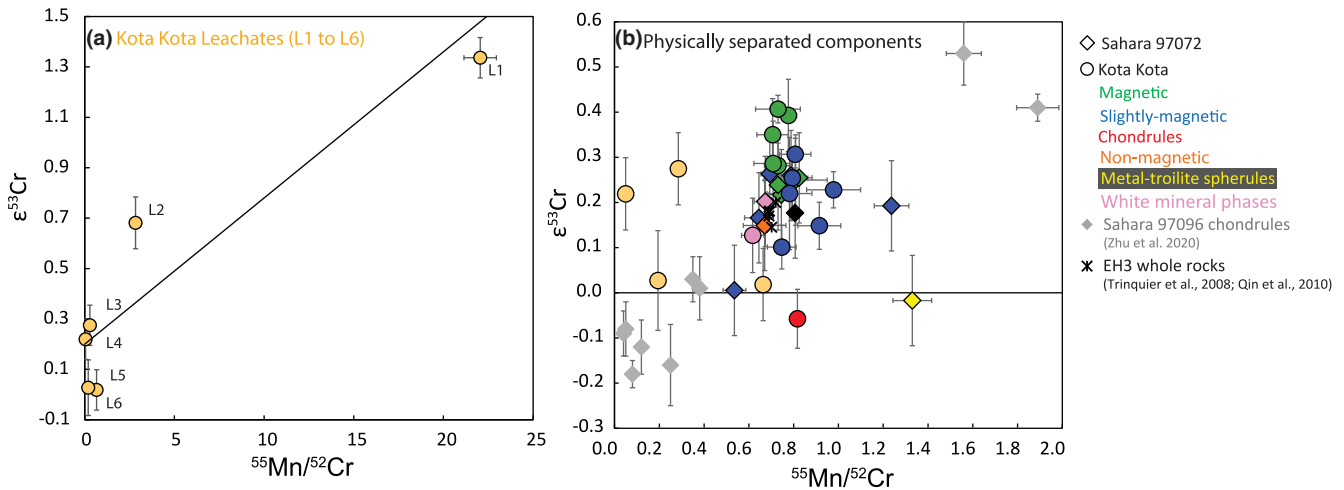
Fig. 3. a) ε^{53}Cr-^{55}Mn/^{52}Cr isochron diagram for the chemical leachates from Kota Kota. b) Physically separated components from Kota Kota and Sahara 97072 show uncorrelated scatter in the isochron diagram. The lack of correlation could be due to redistribution of Mn during terrestrial weathering or during late parent body processes (e.g., impact heating). The internal errorchron of Kota Kota leachates yields an apparent age of 12.6 Myr after the formation of the solar system (equivalent to an age of 4555 ± 2 Ma), assuming an initial ^{53}Mn/^{55}Mn of 6.28 × 10^{-6} at 4567 Ma (Trinquier et al., 2008). The relatively young age may reflect local redistribution of sulfide-hosted Mn by impacts or other processes on the parent body of the EH3 chondrites. (Color figure can be viewed at wileyonlinelibrary.com.)

abundances of Fe and Cr. These discrepancies between observed and expected variations indicate that the variation of Cr isotopes in EH3 chondrites is difficult to explain by heterogeneous mixing of trace fractions of presolar grains or preferential thermal destruction of such grains.

ε^{54}Cr-Fe/Cr Variations in Solar System Objects

For a better understanding of the origin of ε^{54}Cr-Fe/Cr variations in EH3 metal, ε^{54}Cr-Fe/Cr variations among different solar system bodies have to be compared. These include chondrites, the acapulcoite and angrite parent bodies, Mars, Vesta, the UPB, and Earth (Table S2). Bodies for which a reliable bulk composition can be determined, including Mars, mean EC, mean OC, acapulcoites, and ureilites, define a linear correlation between ε^{54}Cr and Fe/Cr with an intercept of ε^{54}Cr = −1.5 at Fe/Cr = 0 (Fig. 2; Fig. S3). The intercept agrees with the less well-defined intercept from the correlation of EH3 metal fractions. The estimates for Vesta are also consistent with this correlation. Little is known about the composition of the core of the angrite parent body (or bodies), and thus, no reliable bulk compositions can be estimated for this body. CCs are uncorrelated in this diagram.

Chondrites

The element and isotope data for the CC groups summarized in Table S2 are from the literature (Göpel et al., 2015; Jarosewich, 1990; Lodders, 2003; Qin et al., 2010; Trinquier et al., 2007). Average values for OC, as well as averages for the individual H, L, and LL chondrite groups were calculated from published data (Kallemeyn et al., 1989; Trinquier et al., 2008; Wasson & Kallemeyn, 1988). The data for individual OC and EC groups are shown in Fig. S3. The OC groups have small variations in average values of ε^{53}Cr and ε^{54}Cr and differ mostly in their Fe/Cr ratios; Mn/Cr ratios display only small variations (Table S2). In OC, the Fe/Cr ratios vary because the different groups show characteristic depletions in Fe-Ni metal from H chondrites (reduced composition, metal is not depleted, Fe/Mg near CI chondrites) to LL chondrites (relatively oxidized, depleted in metal, sub-CI chondritic Fe/Mg).

The enstatite chondrite groups, EL3 and EH3, have similar ε^{53}Cr and ε^{54}Cr, but differ in their Mn/Cr and Fe/Cr (Jarosewich, 1990; Mougel et al., 2018; Qin et al., 2010; Trinquier et al., 2007; Wasson & Kallemeyn, 1988; Weeks & Sears, 1985). The EH chondrites have high Fe/Cr because they are enriched in Fe-Ni metal (supra-CI chondritic Fe/Mg) compared to EL chondrites (Wasson & Kallemeyn, 1988). EH chondrites are also more enriched in moderately volatile elements like Mn than EL chondrites, resulting in a higher Mn/Cr (Wasson & Kallemeyn, 1988).

The data suggest that EH3 chondrites may have a slightly higher ε^{53}Cr than EL3 chondrites (Qin et al., 2010; Trinquier et al., 2008), which is consistent with a higher Mn/Cr of EH chondrites compared to EL chondrites (Wasson & Kallemeyn, 1988). Because the different EC groups differ in their Fe/Cr and Mn/Cr

ratios, but show very similar ε^{54}Cr, it is plausible that the processes that fractionated the elements between the different EC groups occurred after the current ε^{54}Cr and ε^{53}Cr values of the bulk rocks were established. Chromium concentrations in EH and EL chondrites are similar, though large variations in Fe concentrations exist between the two groups (Wasson & Kallemeyn, 1988). Therefore, the Fe/Cr ratio can change significantly due to small variations in the Fe-Ni metal abundances. For instance, if Fe-Ni metal (90% Fe) containing 400 ppm Cr (Qin et al., 2010) is added to EL3 chondrites (or removed from EH chondrites), then only 1% of such metal grains are needed to change the Fe/Cr ratio from 70 (average EL chondrites) to 90 (average EH chondrites). Therefore, such a process can efficiently fractionate the Fe/Cr ratio, but not significant enough to change the overall Cr isotope budget of the components of EH chondrites, because variations in ε^{53}Cr and ε^{54}Cr values will be in the range of analytical uncertainties. Because of the differences in redox conditions, different Fe-Ni metal abundances, volatile element concentrations, as well as O and Cr isotope compositions of the different chondrite groups (Scott & Krot, 2003; Wasson & Kallemeyn, 1988), it is generally accepted that the element fractionation of chondrite groups occurred in the nebular domains from which the different meteorite parent bodies accreted (Warren, 2011; Wasson & Kallemeyn, 1988). The chemical fractionations that are recorded in the meteorites are inherited from their individual components (mostly chondrules and matrix) and thus were caused either by solid–melt–gas interactions during chondrule formation or similar processes involving dust precursors of chondrules (Chaussidon et al., 2008; Friend et al., 2016). As these processes typically occurred within the first 2–3 Myr of solar system formation (Pape et al. [2019] and references therein), this time scale would define the maximum possible duration of the processes that established the ε^{54}Cr and ε^{53}Cr compositions of chondrites. The mean values for OC and EC average out the chemical heterogeneity induced by fractionation processes in nebular domains. This may be the reason why average values for OC and EC result in smaller scatter in Fig. 2a compared to the case when the individual groups of OC and EC are used (Fig. S3).

Acapulcoite and Angrite Parent Bodies

Acapulcoites are primitive achondrites of broadly chondritic composition. They show evidence for partial melting and incipient metal–sulfide–silicate segregation on the parent body (McCoy, 1994). Their Cr content is highly variable (Zipfel & Palme, 1994). Based on the relatively uniform concentrations of K and Th, indicating no loss or gain of partial silicate melt from the acapulcoite parent body, it is assumed that the average Cr content of acapulcoites is representative for the acapulcoite parent body (Zipfel & Palme, 1994). A low average Fe/Cr = 43 and ε^{54}Cr = -0.7 ± 0.1 suggest low Fe abundance and a different source of Cr isotopes compared to chondrites.

Angrites are basic igneous rocks from the crust of a differentiated parent body (Weiss et al., 2008). The bulk composition of the angrite parent body (APB) is not well constrained. Its origin and detailed differentiation history are still debated (Wänke & Dreibus, 1994; Zhu, Moynier, et al., 2019). Therefore, Fe/Cr and Mn/Cr ratios of the APB cannot reliably be determined. Basaltic angrites are depleted in Cr by a factor of 10 compared to CI chondrites (Sanloup et al., 1999), whereas Cr contents and Fe/Cr and Mn/Cr ratios of plutonic angrites are similar to chondrites. Angrites are relatively oxidized with estimated fO$_2$ values ranging from the iron–wustite (IW) buffer to several log units above it (Brett et al., 1977; Kuehner & Irving, 2007; McKay et al., 1994). Thus, it is expected that the Cr content in the silicate part of the APB is relatively high, because only a smaller fraction of Cr partitioned into the core. This is consistent with the high Cr abundances in plutonic angrites with abundances of a few 1000 µg g^{-1}. Here, it is assumed that the Fe/Cr and Mn/Cr ratios of the APB are similar to those of CV chondrites. This assumption is consistent with the siderophile element depletion pattern and core formation models of angrites (Steenstra et al., 2017).

Mars

Different compositions have been proposed for bulk Mars. Some are based on Shergotty/Nakhla/Chaussigny meteorites and others assume, based on isotope compositions and element abundances, that Mars comprises a mixture of materials with different chondritic compositions (Lodders & Fegley, 1997; Sanloup et al., 1999; Taylor, 2013; Wänke & Dreibus, 1994; Yoshizaki & McDonough, 2020). The various estimates for the Fe, Mn, and Cr concentrations for bulk silicate Mars differ by up to 16%, 43%, and 67%, respectively. This makes it difficult to derive reliable estimates for the Fe/Cr and Mn/Cr values for bulk Mars. The present study uses the average Fe, Mn, and Cr concentrations reported in the majority of the models (Lodders & Fegley, 1997; Sanloup et al., 1999; Taylor, 2013; Wänke & Dreibus, 1994).

Vesta

Estimates of the bulk silicate composition of Vesta (Fe/Cr = 19, Mn/Cr = 0.55) were derived from HED meteorites (Dreibus & Wänke, 1980). The estimated bulk composition of Vesta mainly depends on the

uncertain core mass of Vesta and on the estimated composition of the core. Estimates of the mass fraction of Vesta's core range from 2% to 50% (Dreibus et al., 1997; Hewins & Newsom, 1988; Morgan et al., 1978; Newsom, 1985; Newsom & Drake, 1982, 1983; Righter & Drake, 1997; Ruzicka et al., 1997; Trønnes et al., 2019). In Fig. 2b, the Fe/Cr ratio of bulk Vesta was calculated for core masses of 10% and 18% (Trønnes et al., 2019). Assuming negligible partitioning of Mn and minor partitioning of Cr into the core of Vesta during the inferred conditions of core formation (i.e., $T = 2000$ K and IW−1, $D_{Cr} < 1$; Budde et al., 2015; Zhu, Sossi, et al., 2019) yields Fe/Cr$_{bulk\ Vesta}$ (10% core) = 37, Fe/Cr$_{bulk\ Vesta}$ (18% core) = 53, and Mn/Cr$_{bulk\ Vesta}$ = 0.55 (assuming the Fe content of the core is 92%; Dreibus et al., 1997). The estimated $\varepsilon^{53}Cr = 0.11 \pm 0.06$ and $\varepsilon^{54}Cr = -0.73 \pm 0.08$ for Vesta are based on analyses of eucrites and diogenites (Birck & Lugmair, 1988; Qin et al., 2010; Trinquier et al., 2007). The bulk composition of Vesta falls on the linear $\varepsilon^{54}Cr$-Fe/Cr correlation line for a mass fraction of Vesta's core between 10% and 14% (Fig. 2b).

Ureilite Parent Body

Ureilites are primitive achondrites. The UPB accreted very early in the solar system history (within 1.6 Myr after CAIs; Budde et al., 2015). An unusually high carbon content of up to 6 wt%, variable noble gas ratios, and O isotopes suggest that ureilites originate from a heterogeneous and partially molten parent body (Scott et al., 1993). The high abundance of highly siderophile elements in ureilites suggests that either extensive metal segregation did not occur in the parent body or the abundances are the result of complex processes involving fractionation of these elements between solid metal, liquid metal, and silicate melt at variable degrees of crystallization (Goodrich, 1992). Therefore, the degree of differentiation of the UPB and its core–mantle ratio cannot be constrained well using existing information. Early studies assumed that the starting composition of the UPB was similar to carbonaceous chondrites (Clayton & Mayeda, 1988). However, the distinct ^{54}Cr isotope composition makes this highly unlikely. If the UPB accreted rapidly from large pebbles (Kurat, 1988), the core fraction could be close to zero and the Fe/Cr ratio of the UPB might be chondritic and similar to Fe/Cr in monomict ureilites (Yamakawa et al., 2010). Alternatively, if the original parent body was shattered by a large impact event with re-accretion of most of the silicates, the relative mass fraction of its core might be similar to the lunar core, that is, 2% (Trønnes et al., 2019). The heliocentric distance of the formation environment of the ureilite parent body (2.8 AU) was estimated based on the $\varepsilon^{54}Cr$

values of ureilites (Yamakawa et al., 2010) and is thus not independently constrained.

Earth

The $\varepsilon^{54}Cr$ of the bulk silicate Earth (BSE = crust + mantle) is by definition 0. The concentrations of Fe, Mn, and Cr in the BSE can be estimated with Fe/Cr$_{BSE}$ = 25.2 and Mn/Cr$_{BSE}$ = 0.42 (Palme & O'Neill, 2014). However, the uncertainties of these estimates are difficult to quantify. McDonough (2003) assumed a maximum of 10% of light elements in Earth's core and CI chondrite-like composition of Fe, Cr, and a volatility depletion trend for the Mn abundance in the Earth and estimated Fe, Mn, and Cr concentrations in the bulk Earth to be 32.0%, 800 µg g^{-1}, and 4700 µg g^{-1}, respectively, which corresponds to Fe/Cr = 68.1 and Mn/Cr = 0.17.

Current accretion models require metal–silicate equilibration during most of the Earth's accretion history; thus, it is reasonable to assume that $\varepsilon^{54}Cr_{core}$ and $\varepsilon^{54}Cr_{BSE}$ are very similar, if not identical. If accretion of the last 10–20% of Earth's mass occurred under disequilibrium conditions and if segregated sulfide or metal melt was derived from more oxidized CC material as suggested by recent accretion models (Rubie et al., 2011, 2015) and other evidence (e.g., Braukmüller et al., 2019; Budde et al., 2019; Mezger et al., 2021), then Earth's core might have a slightly different $\varepsilon^{54}Cr$ than the BSE. However, because Cr is less siderophile at higher fO_2 (Chabot & Agee, 2003; Corgne et al., 2008), the BSE still contains a significant amount of Cr leading to only a minor effect on the Cr isotopes from late accreted material.

Although $\varepsilon^{54}Cr$ of the BSE is known, the specific Fe/Cr of the core and the bulk Earth are somewhat uncertain. For this reason, two endmember scenarios are considered. First, Earth may have a CI chondrite-like Fe/Cr near 70 (Lodders et al., 2009), as suggested by McDonough (2003). Assuming such an Fe/Cr composition, Earth would lie considerably off the $\varepsilon^{54}Cr$-Fe/Cr correlation line, which could indicate that the Earth contains significant material with a higher $\varepsilon^{54}Cr$ such as volatile-rich carbonaceous chondrites. Various lines of evidence suggest that Earth accreted from a few % up to 10% of volatile element-enriched CC-like material during the late stages of accretion (Braukmüller et al., 2019; Budde et al., 2019; Marty, 2012; Mezger et al., 2021; Schönbächler et al., 2010). The position of the modern Earth in Fig. 2b might be explained if the proto-Earth had a different $\varepsilon^{54}Cr$ than the present Earth (vertical blue line intersecting the correlation line of Fig. 2b at $\varepsilon^{54}Cr = -0.3$). If correct, the Fe/Cr (68–71) and $\varepsilon^{54}Cr$ (−0.3) of such a putative proto-Earth composition can be obtained by subtracting

15% CI chondrite-like material from the modern bulk Earth (Table S2).

Second, reduced density constraints (e.g., Stacey, 2005) and mass balance arguments for major element abundances in BSE and plausible core compositions suggest that Earth has an excess of Fe relative to Mg compared to CI and most other chondrites (e.g., McDonough, 2003; Palme & O'Neill, 2014). Therefore, another option would be that the bulk Earth has a higher Fe/Cr than the CI chondrite value. Assuming Fe/Cr of the bulk Earth is 80, then the Earth lies on the ε^{54}Cr and Fe/Cr correlation line and the bulk Earth has similar ε^{54}Cr and Fe/Cr as average enstatite chondrites (Fig. 2b). If up to ~3% of CI chondrite material (e.g., Albarède, 2009; Marty, 2012) was added to the Earth during accretion, then bulk Earth and proto-Earth both fall on the ε^{54}Cr-Fe/Cr correlation (Fig. 2b).

The Effect of Early Irradiation of Dust and Pebbles on Cr Isotope Variation in the Inner Solar System

Figure 2a shows that ε^{54}Cr correlates with Fe/Cr in EH3 magnetic fractions and in most objects from the inner solar system. If isotope variations correlate with major element compositions, models that mix or destroy presolar grains due to transport and heating processes in the nebula must explain collateral effects on the bulk chemical composition of bodies in the inner solar system. The slopes of the ε^{53}Cr-ε^{54}Cr correlation and of ε^{53}Cr and ε^{54}Cr versus Fe/Cr in the magnetic fractions of the EH3 chondrites and other solar system objects possibly indicate an origin by either irradiation and/or mixing of Fe-^{54}Cr-rich phases in different domains of the solar nebula.

Iron and Ni are the main target elements for spallogenic Cr and irradiation results in a characteristic isotope ratio of ε^{54}Cr/ε^{53}Cr ~ 3.6–3.9 for pure Fe and 1.4 for pure Ni targets (Liu et al., 2019). The slope of the magnetic fractions from Sahara 97072 and Kota Kota is similar within the uncertainty to the theoretical slope (3.6) produced by irradiation of pure Fe (Fig. 1). Correlated variations of ε^{53}Cr and ε^{54}Cr are known from iron meteorites, and they can be explained by coupled production of ^{53}Cr and ^{54}Cr by the interaction of galactic cosmic rays (GCR) with Fe, Cr, and Ni (Liu et al., 2019). Therefore, the correlation between ε^{54}Cr, ε^{53}Cr, and Fe/Cr in magnetic separates of EH3 chondrites and the ε^{54}Cr-Fe/Cr correlation in other inner solar system bodies (Fig. 2) suggest that variations in ε^{54}Cr and ε^{53}Cr in these materials could also result from irradiation.

Irradiation by solar energetic particles is a potential source for some long- and short-lived nuclides in refractory inclusions in chondrites (Goswami et al., 2001; McKeegan et al., 2000). Cosmogenic ^{53}Cr and ^{54}Cr variations might have been produced during different times and in different environments during the evolution of the solar system. First, similar to ^{10}Be, irradiation of dust grains in molecular clouds by GCR particles can cause heterogeneous production of ^{53}Cr and ^{54}Cr in the molecular cloud (Desch et al., 2004). The average size of dust in the molecular cloud precursor of the solar system was a few tens of μm only (Blitz & Shu, 1980). Due to this small size and the low dust/gas ratio, most interaction of GCR with such dust grains is elastic, and thus, based on model calculations (Hirtz, 2019), it is not possible to achieve the measured ε^{54}Cr and ε^{53}Cr in the presumed lifetime of the molecular cloud which was only a few tens of Myr. Second, irradiation of dust grains and pebbles in the nebula by solar energetic particles and/or GCR during the T-Tauri phase of the young Sun (Goswami et al., 2001; Lee, 1978) may have modified the abundances of neutron-rich isotopes. Third, irradiation of meteorites and surfaces of bodies without an atmosphere (e.g., on the Moon) by solar energetic particles and GCR occurred during the later history (Lal & Venkatavaradan, 1967; Reedy et al., 1983). Cosmogenic contributions to Cr isotopes generated by the irradiation of meteoroids are relatively easy to constrain using exposure ages and Fe/Cr ratios (Trinquier et al., 2007). Because of the typically low exposure ages of the EH chondrites (Patzer & Schultz, 2001), contributions from late irradiation result only in negligible changes in ε^{53}Cr and ε^{54}Cr of the components (Fig. S1).

Therefore, the irradiation of early solar system dust and pebbles by solar energetic particles remains as the most plausible process to account for the observed neutron-rich isotopic anomalies in ^{54}Cr and their coupling with the Fe/Cr ratio in inner solar system materials (Fig. 2). The slope of the ε^{54}Cr- ε^{53}Cr correlation of magnetic fractions of EH3 chondrites (Fig. 1) is consistent with this process.

The irradiation of dust and pebbles by enhanced solar energetic particle fluxes in the early solar system can be modeled to evaluate plausible irradiation conditions that might produce the observed ε^{54}Cr and ε^{53}Cr as a function of heliocentric distance. For the model calculations, dust and pebbles with CI-chondrite-like concentrations of Ti, V, Cr, Mn, and Fe are considered as the main targets for irradiation in the solar nebula. For the chemistry considered and the size and dimensions of the irradiated targets, Fe is the most relevant target element for spallogenic production of Cr isotopes by solar energetic particles (SEP) and GCR, whereas contributions from Cr, Mn, V, Ni, and Ca are only minor.

The production rates (atom/g/s) for product isotope $X_h(P)$ can be calculated via:

$$X_h(P) = \left(N_A \sum_i C_i A_i^{-1} \sum_k \int_0^\infty \sigma_{h,i,k}(E) J_k(E,\ P) dE\right)_{SEP}$$
$$+ \left(N_A \sum_i C_i A_i^{-1} \sum_k \int_0^\infty \sigma_{h,i,k}(E) J_k(E,\ P) dE\right)_{GCR}.$$

(2)

N_A = Avogadro's number ($6.02214076 \times 10^{23}$ mol^{-1})
C_i = Concentration of the target element i [g/g]
A_i = Mass number of target element i
$\sigma_{h,i,k}(E)$ = Excitation function for the production of nuclide h from target element i by projectile of type k. The cross sections are functions of projectile energy E
$J_k(E,\ P)$ = Differential flux density of projectile type k
P = Power law index of the spectral shape

The spectral shape for solar particle events is assumed to be proportional to E^{-P}, with P the power-law index and the energy as energy per nucleon. For solar particle events, gradual events with $P = 2.7$ are distinguished from gradual events with $P = 4.0$ (Leya et al., 2003). The H/He ratios for gradual and impulsive events are 300 and 10, respectively (Leya et al., 2003). The ^{3}He/^{4}He ratios for gradual and impulsive events are 4×10^{-4} and 1, respectively (Leya et al., 2003). The particle fluence (atoms/cm^2) is assumed to be 9.95×10^{22} (Hirtz, 2019). For the target composition of the dust and pebbles, a CI-chondrite-like chemical composition is assumed for the relevant elements (Lodders, 2003). The initial ε^{54}Cr prior to irradiation is considered to be $= -1.5$ (intercept of the correlation ε^{54}Cr versus Fe/Cr at Fe $= 0$ in Fig. 2). For the modeling of production rates of cosmogenic nuclides, the CosmicTransmutation code was used, which is a new model developed at the University of Bern based on the Geant4 toolkit. The physics list used is FTFP_INCLXX_HP (Hirtz, 2019).

For GCRs, the main interacting particles are protons and alpha particles in the energy range 10 MeV/nucleon to 100 GeV/nucleon. The particle fluxes used in the calculations for protons are:

$$J_P(T,\ M) = c_P \times \frac{T(T + 2m_P c^2)(T + x + M)^{-2.65}}{(T + M)(T + 2m_p c^2 + M)}$$

(3)

with T the kinetic energy, M the solar modulation potential ($M = 1000$ MeV in our calculations), c_p is proton flux, m_p the rest mass of the proton, and $m_p c^2$ is proton rest energy. The factor x(the proton flux of specific energy from outside the solar system) is defined as:

$$x = 780 \times e^{-2.5 \times 10^{-4} \times T}$$

(4)

For a flux in the unit [particle m^{-2} s^{-1} sr^{-1} MeV^{-1}], the parameters T, M, x, and $m_p c^2$ must be expressed in MeV and the normalization factor is $c_p = 10^9$.

The alpha-particles are described via:

$$J_{\alpha(T,K)} = \frac{c_\alpha \times T^K \times (T + 2m_a c^2)}{(T + 700)(T + 2m_a c^2 + 700)(T + 312500 T^{-2.5} + 700)^{1.65+K}}$$

(5)

where T = the kinetic energy per nucleon [MeV/nucleon] and $c_\alpha = 5.5 \times 10^7$ for a flux in the unit [particle m^{-2} s^{-1} sr^{-1} (MeV/nucleon)$^{-1}$]. The parameter K considers the solar activity and is based on the solar modulation parameter M for protons via:

$$K = (1.786 \times 10^{-3} \times M) - 0.1323$$

(6)

The solar fluence is temporally variable, especially in the early solar system. Recent observations of T-Tauri stars in the mass range 0.7–1.4 solar masses located in clusters of the Orion nebula show that during a stellar T-Tauri phase, the particle flux could be temporally up to 10^5 times higher than the current flux of the Sun (Feigelson et al., 2002).

The contribution to irradiation-produced ^{54}Cr and ^{53}Cr due to GCR spallation reactions on Fe targets is very small (e.g., the production of Cr isotopes due to GCR spallation reactions on an Fe-target is <5% of the Cr isotopes produced by SEP spallation reactions on an Fe-target). However, we also added a GCR contribution to the final cosmogenic Cr isotope (in Fig. 3) plots because it exists. Excluding GCR contributions will not make any significant difference.

The irradiation-produced slope of ^{54}Cr/^{53}Cr is mainly dependent on the flux and energy of the interacting particles and the concentrations of target elements. For a particular model simulation, we assume that the particle fluxes (mainly protons and ^{3}He) from the SEP spectrum are the same as for GCR. The main difference between SEP and GCR spectra is the different energy distributions of the particles. For constant target compositions, the differences in energy of the particles mainly result in a change of the concentrations of all nuclides produced during irradiation, but not the nuclide production ratios. Therefore, the ^{54}Cr/^{53}Cr ratio and slope remain same for both SEP and GCR irradiation at otherwise constant boundary conditions.

The presence of gas in the early solar system has an impact on the irradiation of dust and can significantly

reduce the yield of spallation reactions in the dust grains either due to absorption of the projectiles, that is, a reduction of the particle fluxes, and/or due to attenuation, that is, the slowing down of projectiles. However, the latter effect can also increase the reaction yield for very low energy products, as can be seen, for example, by increasing reaction yields with increasing shielding in pebbles. The simulations show that the main changes caused by solar cosmic rays propagating through a gas before entering the dust grain is simply a reduction in the particle flux. This effect can be compensated by either assuming a higher activity of the early Sun and/or a longer irradiation time. For stable products, that is, ^{53}Cr and ^{54}Cr, the total irradiation effect is proportional to flux density times irradiation time and a reduction of one value can easily be compensated by a respective increase of the other value. There is a relevant difference between an irradiation with and without surrounding gas. The irradiation with surrounding gas creates a low energetic neutron background, which might be relevant for some special applications.

Attenuation effects are expected to be low in the modeled scenario. The majority of the solar/nebular gas comprises H and He. The high temperatures in the inner solar system likely resulted in a depletion of, for example, H, He, and N close to the Sun, that is, most of the gas was moving toward the outer solar system or fell back into the Sun and caused nonuniform gas densities in the early solar nebula (Haghighipour & Boss, 2003). Because there are many possible and poorly constrained scenarios and to keep the model simple, the attenuation effects in the gas for the production of cosmogenic nuclides were not considered. However, different scenarios for an irradiation of dust and pebbles in the solar nebula may be relevant.

Case 1—Irradiation of Dust Grains at Different Heliocentric Distance

The ε^{54}Cr values of Vesta and the ureilite parent body/ies are consistent with the irradiation of 1 mm-sized dust at ~2.3 and ~2.8 AU, respectively (Fig. 4). Assuming Mars formed near 1.5 AU, its ε^{54}Cr indicates irradiation of predominantly 1 cm-sized pebbles. Assuming the Cr isotope composition of the Earth is represented by the bulk silicate Earth (ε^{54}Cr$_{BSE}$ ~0, see supporting information) and the contribution of CI-like material is no more than a few % (Fig. 2), its ε^{54}Cr can be reproduced by irradiation of pebbles having an average size of 10 cm (Fig. 4). This result is consistent with the predicted larger size of dust grains and pebbles and their rapid growth during irradiation in the inner compared to the outer solar nebula (Nakagawa et al., 1986).

Together with Mars and some achondrites, the mean values of ECs and OCs define the ε^{54}Cr −Fe/Cr correlation line of objects in the inner solar system (Fig. 2). The EH and EL chondrite groups show different Fe/Cr ratios at constant ε^{54}Cr (Qin et al., 2010; Trinquier et al., 2007; Wasson & Kallemeyn, 1988) (Fig. S3), possibly indicating fractionation of Fe/Cr in enstatite chondrites due to the variable presence of MTS metal. The high ε^{54}Cr values for enstatite chondrites and the Earth are consistent with an origin in the innermost solar system at <1 AU (Figs. 2 and 3). Mars has a lower ε^{54}Cr, indicating that it may contain a larger proportion of less irradiated material.

Case 2—Irradiation of Dust Grains Near the Sun and Subsequent Transport to Different Heliocentric Distances

This scenario is in principle similar to the model advocated for the formation and transport of CAIs by X-winds (Shu et al., 1997). If the cosmogenic ^{54}Cr was produced near the Sun and if dust grains were transported outward, then the variations in ε^{54}Cr seen in inner solar system objects require concentrations of only 0.00014% of irradiation-produced Cr to the ureilite parent body and of 0.0004% of irradiation-produced Cr (calculated from the difference between ^{54}Cr/^{52}Cr ratio produced by the irradiation and observed in the inner solar system objects) to the EC parent body (Fig. 5). Consequently, the amount of irradiation-produced material required to explain the inner solar system isotope data is very low. Thus, this model faces similar problems as presolar grains, because the mass fractions of the irradiated components are so small that they do not affect Fe/Cr variations and are not consistent with the observed correlations shown in Fig. 2.

Case 3—Irradiation as a Function of Heliocentric Distance, Time, and Mixing During Accretion

The general ε^{54}Cr-Fe/Cr correlation of inner solar system objects in Fig. 2 might be the result of a combination of variable irradiation intensities as a function of heliocentric distance (and irradiation time) and later mixing of NC planetesimals and embryos that formed in the inner solar system (e.g., Kruijer et al., 2017; Warren, 2011). Some bodies of the inner solar system define a correlation between ε^{54}Cr, Fe/Cr, and heliocentric distance, notably ECs (which are thought to be derived from <1 AU, Clayton et al., 1984; Larimer & Bartholomay, 1979; Mason, 1966), Earth, Mars, OCs, and Vesta (Fig. 2). For other bodies (ureilites, acapulcoites, angrite parent bodies), the relationship with heliocentric distance is unclear. Because the trend of inner solar system objects in Fig. 2 is well defined,
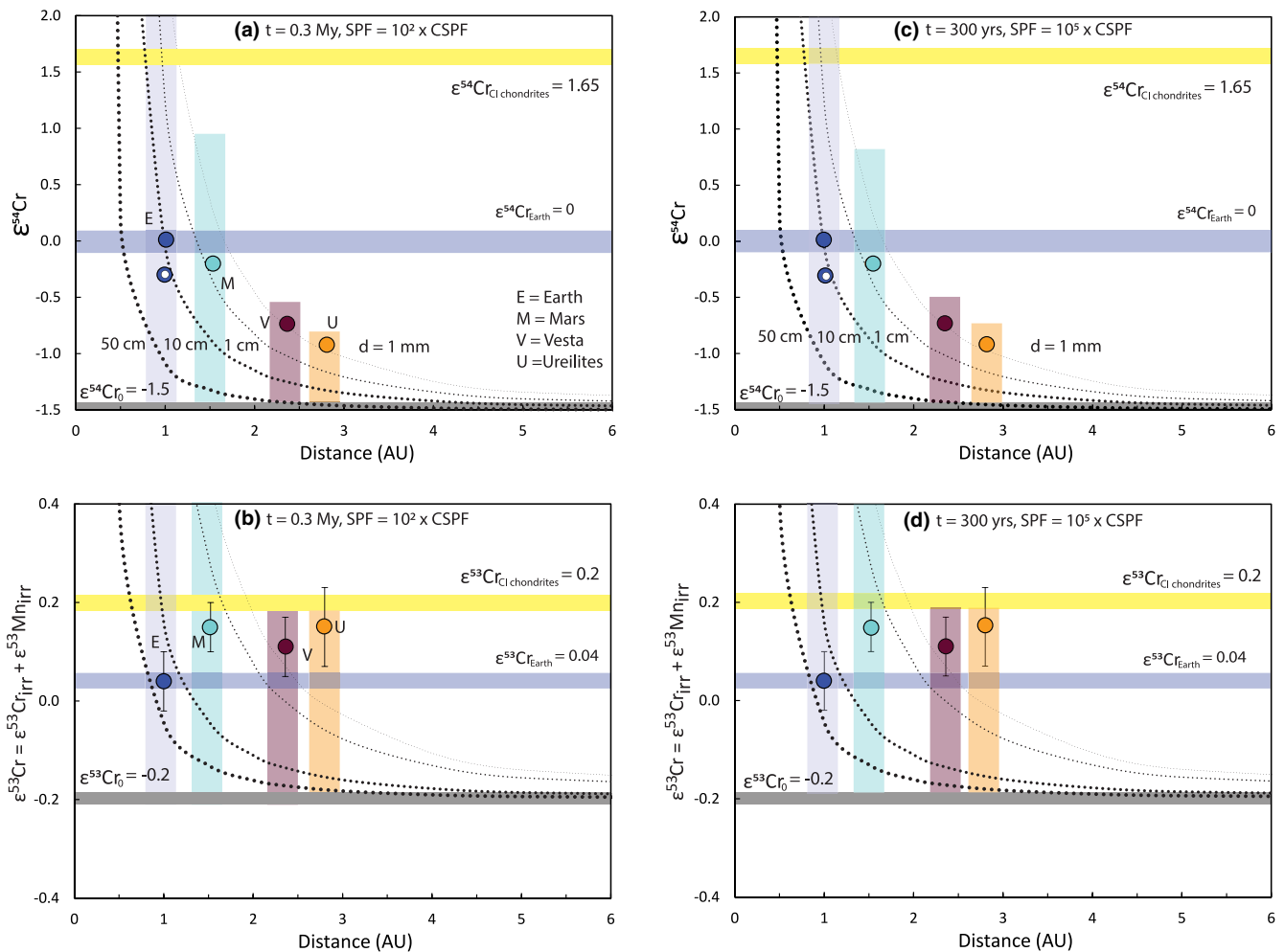
Fig. 4. a) $\varepsilon^{54}Cr$ versus heliocentric distance (AU) in inner solar system objects together with results of irradiation models. b) $\varepsilon^{53}Cr$ versus heliocentric distance in inner solar system objects. The dotted curves show the modeled variation of $\varepsilon^{54}Cr$ in dust and pebbles with CI-chondrite like mass fractions and elemental ratios of Fe, Cr, Mn, Ti, and V due to irradiation by SEP and GCR for an irradiation time (t_{irr}) of 0.3 Myr and a solar particle flux (SPF) 10^2 times the current solar particle flux (CSPF, see supporting information for details). The modelled diameters of dust and pebbles are 1 mm, 1 cm, 10 cm, and 50 cm; (c) and (d) are similar to (a) and (b) but with t_{irr} of 300 yr and for a solar particle flux 10^5 times the current solar particle flux. Horizontal bars reflect the specified compositions. (Color figure can be viewed at wileyonlinelibrary.com.)

there is only limited room for late admixing of CC-like material to inner solar system objects. However, mixing by planetary accretion of material that originated from different heliocentric distances in the inner solar system is a possibility. For instance, the position of Mars in Fig. 2 implies the presence of a significant fraction of non-EC-like inner solar system material in this planet. Earth's proximity to the $\varepsilon^{54}Cr$ value of EC does not necessarily mean that it mostly comprises EC material (e.g., Dauphas, 2017; Warren, 2011). Accretion of variably irradiated material, including more strongly and weakly irradiated material than EC, is a possibility. Several studies have shown that a predominant EC component is inconsistent with the chemical and stable Si isotope composition of the Earth (Fitoussi &

Bourdon, 2012; Kadlag et al., 2019; Palme & O'Neill, 2014; and references therein). However, since the true irradiated endmember compositions in Earth and Mars are currently unknown, mixing proportions are poorly constrained.

The $\varepsilon^{54}Cr$-Fe/Cr correlation in solar system objects favors case 1 or case 3 over case 2. Dependence of $\varepsilon^{54}Cr$ on the Fe/Cr ratio also suggests significant loss of Cr from inner solar system objects (mainly from ECs, Earth, and Mars). Part of the Cr could have either been lost into the Sun or moved to higher heliocentric distance due to higher temperatures closer to the Sun. Variable proportions of irradiation-produced Cr (^{54}Cr-enriched) could have been added later to the remaining (^{54}Cr-depleted) Cr in the inner solar system.
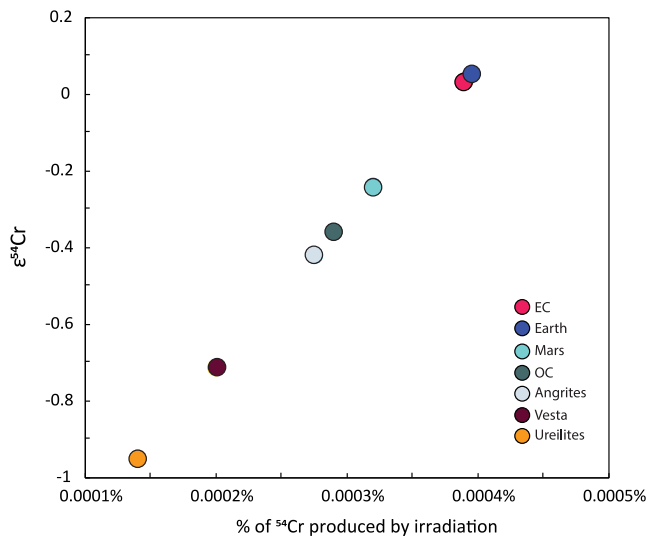
Fig. 5. ε^{54}Cr versus percent of irradiated dust grains added to the formation regions of inner solar system objects. The variation of ε^{54}Cr in inner solar system objects can be explained by accretion of 0.0004% of pure spallation produced Cr to the EH chondrite parent body or 0.00014% to the UPB. For the calculation we assumed a homogeneous initial ε^{54}Cr of −1.5. (Color figure can be viewed at wileyonlinelibrary.com.)

Origin of the Variation of ^{53}Cr in the Inner Solar System

The variation in the ^{53}Mn/^{55}Mn ratio at different heliocentric distance and for different pebble sizes is shown in Figs. 4b and 4d. If the ε^{54}Cr variation in inner solar system objects is predominantly controlled by the irradiation of dust and pebbles (Fig. 3), ε^{53}Cr might also be affected. However, the calculated variation in irradiation-produced ^{53}Cr is very low, that is, it is less than typical measurement uncertainties on ε^{53}Cr (Fig. 4). In contrast, irradiation-produced ^{53}Mn can yield up to 1.5ε units of radiogenic ε^{53}Cr in 1 mm-sized pebbles in the formation region of the terrestrial planets (Table S3). Therefore, spallation-produced ^{53}Cr is factors of 10–100 lower than the production from ^{53}Mn and can therefore be neglected (Table S3). Consequently, if Fe, Mn, Cr separation occurred early in the solar nebula, that is, within the lifetime of ^{53}Mn, then the expected variation of ε^{53}Cr in inner solar system objects would not be a function of heliocentric distance (Fig. 3b), but only a function of the Mn/Cr ratios, because variations in ε^{53}Cr would almost entirely be due to radioactive decay of ^{53}Mn. The range of slopes of ^{54}Cr versus ^{53}Cr (Fig. 1) in metal-rich and metal-poor physically separated fractions of Kota Kota and Sahara 97072 and the decoupled ^{54}Cr-^{53}Cr variations in leachates (mainly L1 and L6) of Kota Kota suggest that the carrier phases of ^{53}Cr and ^{54}Cr are different and may have different volatilities. The

early efficient separation of ^{53}Mn from Fe-rich metal grains, which carry the irradiation signal, requires that during the period of irradiation, temperatures in the inner nebular disk must have been significantly above the half mass condensation temperature of Mn (1123 K, Wood et al., 2019). Alternatively, effective evaporation and separation of Mn from Fe-rich phases might have occurred during repeated evaporation/condensation cycles or prolonged high temperature episodes in the inner solar nebula. Decoupling of ^{54}Cr and ^{53}Cr on the mineral scale occurred because the metals that carry the irradiation signal did not evaporate, whereas Mn evaporated and recondensed into sulfides (in enstatite chondrites) and silicates (in ordinary chondrites). Consequently, if Mn-Cr fractionation occurred due to volatilization of Mn during or after irradiation of dust and pebbles, a correlation of ε^{53}Cr with Mn/Cr ratios in bulk inner solar system materials is expected. These irradiation and evaporation processes likely occurred before the separation of the protoplanetary disk into NC and CC reservoirs, because both NC and CC objects yield evidence for a nearly homogeneous distribution of ^{53}Mn in their formation areas (Göpel et al., 2015; Lugmair & Shukolyukov; 1998; Qin et al., 2010; Trinquier et al., 2008). The possible role and timing of supernova material injection into the region where CCs formed warrant further investigation in the light of the results from the present study.

SUMMARY AND CONCLUSIONS

The ε^{54}Cr variations among different inner solar system objects and among different components of chondrites can be explained by the incorporation of dust grains and pebbles with variable degrees of irradiation. Some of these components (e.g., MTS) may have formed in different environments (Kadlag et al., 2019) compared to the main components of the EH chondrite parent body. The lower ε^{53}Cr and ε^{54}Cr in the MTS fraction from an EC suggest shielding of bigger metal grains, possibly in an early formed planetary body, that was disrupted during collision and partly re-accreted.

Heterogeneity of ^{54}Cr and a homogeneous distribution of ^{53}Mn in the solar system suggest that after the irradiation (e.g., ~300 yr of effective irradiation time), nebular disk temperatures in areas where condensation occurred were lower than the half mass condensation temperature of Cr (1291 K) and higher than the half mass condensation temperature of Mn (i.e., 1123 K, Wood et al., 2019). In addition, efficient mixing of gas in the solar system must have occurred to homogenize most of the spallation-produced ^{53}Mn and to erase any nucleosynthetic isotope

anomalies in other volatile elements (Moynier et al., 2009; Trinquier et al., 2008; Vollstaedt et al., 2020). Because ε^{54}Cr correlates with variations of other neutron-rich nuclides in inner solar system objects (e.g., Schiller et al., 2018; Trinquier et al., 2009; Warren, 2011), the isotope effects in ^{48}Ca, ^{50}Ti, ^{64}Ni, and possibly other neutron-rich isotopes in the inner solar system may also be controlled by solar energetic particles. The strong positive correlation of ε^{54}Cr with mass-independent Δ^{17}O variations in NC meteorites (Trinquier et al., 2007) could be a consequence of collateral early enhanced UV irradiation from the active proto-Sun. Thus, irradiation-induced isotope anomalies of the relatively refractory element Cr, and possibly also Ti and Ca, but not in volatile elements in the inner solar system may reflect higher temperatures ($T_{cond} \geq 1300$ K) after nuclide production during the irradiation of relatively refractory dust. The preserved correlation between ε^{54}Cr, Fe/Cr, and the presumed heliocentric distance of at least some inner solar system objects implies that mixing of variably irradiated dust may have been limited to relatively narrow feeding zones of the accreting objects (see also Sugiura & Fujiya, 2014). The different masses of the bodies and the inferred isotopic-chemical gradient may comprise remnants of a multi-ring structure of mass distribution in the early inner solar system. These variations were likely established within the first few hundred thousand years in the inner solar system as an effect of irradiation, volatilization of a fraction of the dust, and homogenization of the gas in the inner solar system.

Data Availability Statement—The data that supports the findings of this study are available in the supplementary material of this article.

Editorial Handling—Dr. Akira Yamaguchi

REFERENCES

Albarède, F. 2009. Volatile Accretion History of the Terrestrial Planets and Dynamic Implications. *Nature* 461: 1227–33.

Birck, J. L., and Allegre, C. J. 1988. Manganese—Chromium Isotope Systematics and the Development of the Early Solar System. *Nature* 331: 579–84.

Birck, J. L., and Lugmair, G. W. 1988. Nickel and Chromium Isotopes in Allende Inclusions. *Earth and Planetary Science Letters* 90: 131–43.

Blitz, L., and Shu, F. H. 1980. The Origin and Lifetime of Giant Molecular Cloud Complexes. *The Astrophysical Journal* 238: 148–57.

Boss, A. P. 2004. Evolution of the Solar Nebula. VI. Mixing and Transport of Isotopic Heterogeneity. *The Astrophysical Journal* 616: 1265–77.

Braukmüller, N., Wombacher, F., Funk, C., and Münker, C. 2019. Earth's Volatile Element Depletion Pattern Inherited from a Carbonaceous Chondrite-Like Source. *Nature Geoscience* 12: 564–8.

Brearley, A. J., and Jones, R. H. 1998. Chondritic Meteorites. In *Planetary Materials*. In Papike, J. J. (Ed.), Reviews in Mineralogy and Geochemistry, vol. 36. Washington, D.C.: Mineralogical Society of America, pp. 3.1–3.38.

Brett, R., Huebner, J. S., and Sato, M. 1977. Measured Oxygen Fugacities of the Angra dos Reis Achondrite as a Function of Temperature. *Earth and Planetary Science Letters* 35: 363–8.

Budde, G., Burkhardt, C., and Kleine, T. 2019. Molybdenum Isotopic Evidence for the Late Accretion of Outer Solar System Material to Earth. *Nature Astronomy* 3: 736–41.

Budde, G., Kruijer, T. S., Fischer-Gödde, M., Irving, A. J., and Kleine, T. 2015. Planetesimal Differentiation Revealed by the Hf–W Systematics of Ureilites. *Earth and Planetary Science Letters* 430: 316–25.

Chabot, N. L., and Agee, C. B. 2003. Core Formation in the Earth and Moon: New Experimental Constraints from V, Cr, and Mn. *Geochimica et Cosmochimica Acta* 67: 2077–91.

Chaussidon, M., Libourel, G., and Krot, A. N. 2008. Oxygen Isotopic Constraints on the Origin of Magnesian Chondrules and on the Gaseous Reservoirs in the Early Solar System. *Geochimica et Cosmochimica Acta* 72: 1924–38.

Clarke, R. S. Jr., Jarosewich, E., Mason, B., Nelen, J., Gomez, M., and Hyde, J. R. 1971. Allende, Mexico, Meteorite Shower. *Smithsonian Contributions to the Earth Sciences*: 1–53.

Clayton, R. N., Mayeda, T. K., and Rubin, A. E. 1984. Oxygen Isotopic Compositions of Enstatite Chondrites and Aubrites. *Journal of Geophysical Research: Solid Earth* 89: C245–9.

Clayton, R. N., and Mayeda, T. K. 1988. Formation of Ureilites by Nebular Processes. *Geochimica et Cosmochimica Acta* 52: 1313–8.

Corgne, A., Keshav, S., Wood, B. J., McDonough, W. F., and Fei, Y. 2008. Metal-Silicate Partitioning and Constraints on Core Composition and Oxygen Fugacity During Earth Accretion. *Geochimica et Cosmochimica Acta* 72: 574–89.

Dauphas, N. 2017. The Isotopic Nature of the Earth's Accreting Material through Time. *Nature* 541: 521–4.

Dauphas, N., Remusat, L., Chen, J. H., Roskosz, M., Papanastassiou, D. A., Stodolna, J., Guan, Y., Ma, C.,

and Eiler, J. M. 2010. Neutron-Rich Chromium Isotope Anomalies in Supernova Nanoparticles. *The Astrophysical Journal* 720: 1577–91.

Desch, S. J., Connolly, H. C. Jr., and Srinivasan, G. 2004. An Interstellar Origin for the Beryllium 10 in Calcium-Rich, Aluminum-Rich Inclusions. *The Astrophysical Journal* 602: 528–42.

Dreibus, G., Bruckner, J., and Wanke, H. 1997. On the Core Mass of the Asteroid Vesta (abstract). *Meteoritics & Planetary Science* 32: A36.

Dreibus, G., and Wänke, H. 1980. The Bulk Composition of the Eucrite Parent Asteroid and its Bearing on Planetary Evolution. *Zeitschrift für Naturforschung A* 35: 204–16.

Fagan, T. J., Krot, A. N., and Keil, K. 2000. Calcium-Aluminum-Rich Inclusions in Enstatite Chondrites (I): Mineralogy and Textures. *Meteoritics & Planetary Science* 35: 771–81.

Feigelson, E. D., Garmire, G. P., and Pravdo, S. H. 2002. Magnetic Flaring in the Pre-Main-Sequence Sun and Implications for the Early Solar System. *The Astrophysical Journal* 572: 335–49.

Fitoussi, C., and Bourdon, B. 2012. Silicon Istope Evidence against an Enstatite Chrondrite Earth. *Science* 335: 1477–80.

Friend, P., Hezel, D. C., and Mucerschi, D. 2016. The Conditions of Chondrule Formation, Part II: Open System. *Geochimica et Cosmochimica Acta* 173: 198–209.

Goodrich, C. A. 1992. Ureilites: A Critical Review. *Meteoritics* 27: 327–52.

Goodrich, C. A., Kita, N. T., Yin, Q.-Z., Sanborn, M. E., Williams, C. D., Nakashima, D., Lane, M. D., and Boyle, S. 2017. Petrogenesis and Provenance of Ungrouped Achondrite Northwest Africa 7325 from Petrology, Trace Elements, Oxygen, Chromium and Titanium Isotopes, and Mid-IR Spectroscopy. *Geochimica et Cosmochimica Acta* 203: 381–403.

Göpel, C., Birck, J. L., Galy, A., Barrat, J. A., and Zanda, B. 2015. Mn–Cr Systematics in Primitive Meteorites: Insights From Mineral Separation and Partial Dissolution. *Geochimica et Cosmochimica Acta* 156: 1–24.

Goswami, J. N., Marhas, K. K., and Sahijpal, S. 2001. Did Solar Energetic Particles Produce the Short-Lived Nuclides Present in the Early Solar System? *The Astrophysical Journal* 549: 1151–9.

Govindaraju, K. 1982. Report (1967–1981) on Four ANRT Rock Reference Samples: Diorite DR-N, Serpentine UB-N, Bauxite BX-N and Disthene DT-N. *Geostandards Newsletter* 6: 91–159.

Haghighipour, N., and Boss, A. P. 2003. On Pressure Gradients and Rapid Migration of Solids in a Nonuniform Solar Nebula. *The Astrophysical Journal* 583: 996–1003.

Hartmann, D., Woosley, S. E., and El Eid, M. F. 1985. Nucleosynthesis in Neutron-Rich Supernova Ejecta. *The Astrophysical Journal* 297: 837–45.

Hewins, R. H., and Newsom, H. E. 1988. Igneous activity in the early Solar System. In Kerridge, J. F. & Matthews, M. S. (Eds.), *Meteorites and the Early Solar System*. Tucson, AZ: University of Arizona Press, pp. 73–101.

Hirtz, J. 2019. *Nuclear Reaction Codes Development for the Particles and Nuclei Production in Meteoroids and Planetary Atmospheres*. PhD thesis, Universität Bern.

Jarosewich, E. 1971. Chemical Analysis of the Murchison Meteorite. *Meteoritics* 6: 49.

Jarosewich, E. 1990. Chemical Analyses of Meteorites: A Compilation of Stony and Iron Meteorite Analyses. *Meteoritics* 25: 323–37.

Kadlag, Y., and Becker, H. 2015. Fractionation of Highly Siderophile and Chalcogen Elements in Components of EH3 Chondrites. *Geochimica et Cosmochimica Acta* 161: 166–87.

Kadlag, Y., Tatzel, M., Frick, D. A., and Becker, H. 2019. The Origin of Unequilibrated EH Chondrites-Constraints From In Situ Analysis of Si Isotopes, Major and Trace Elements in Silicates and Metal. *Geochimica et Cosmochimica Acta* 267: 300–21.

Kallemeyn, G. W., Rubin, A. E., Wang, D., and Wasson, J. T. 1989. Ordinary Chondrites: Bulk Compositions, Classification, Lithophile-Element Fractionations and Composition-Petrographic Type Relationships. *Geochimica et Cosmochimica Acta* 53: 2747–67.

Kallemeyn, G. W., and Wasson, J. T. 1981. The Compositional Classification of Chondrites—I. The Carbonaceous Chondrite Groups. *Geochimica et Cosmochimica Acta* 45: 1217–30.

Kruijer, T. S., Burkhardt, C., Budde, G., and Kleine, T. 2017. Age of Jupiter Inferred from the Distinct Genetics and Formation Times of Meteorites. *Proceedings of the National Academy of Sciences* 114: 6712–6.

Kuehner, S. M., and Irving, A. J. 2007. Primary Ferric Iron-Bearing Rhönite in Plutonic Igneous Angrite NWA 4590: Implications for Redox Conditions on the Angrite Parent Body. AGUFM P41A-0219.

Kurat, G. 1988. Primitive Meteorites: An Attempt Towards Unification. *Philosophical Transactions of the Royal Society of London, Series A, Mathematical and Physical Sciences* 325: 459–82.

Lal, D., and Venkatavaradan, V. S. 1967. Activation of Cosmic Dust by Cosmic-Ray Particles. *Earth and Planetary Science Letters* 3: 299–310.

Larimer, J. W., and Bartholomay, M. 1979. The Role of Carbon and Oxygen in Cosmic Gases: Some Applications to the Chemistry and Mineralogy of Enstatite Chondrites. *Geochimica et Cosmochimica Acta* 43: 1455–66.

Lee, T. 1978. A Local Proton Irradiation Model for Isotopic Anomalies in the Solar System. *The Astrophysical Journal* 224: 217–26.

Leya, I., Halliday, A. N., and Wieler, R. 2003. The predictable Collateral Consequences of Nucleosynthesis by Spallation Reactions in the Early Solar System. *The Astrophysical Journal* 594: 605–16.

Liu, J., Qin, L., Xia, J., Carlson, R. W., Leya, I., Dauphas, N., and He, Y. 2019. Cosmogenic Effects on Chromium Isotopes in Meteorites. *Geochimica et Cosmochimica Acta* 251: 73–86.

Lodders, K. 2003. Solar System Abundances and Condensation Temperatures of the Elements. *The Astrophysical Journal* 591: 1220–47.

Lodders, K., and Fegley, B. 1997. An Oxygen Isotope Model for the Composition of Mars. *Icarus* 126: 373–94.

Lodders, K., Palme, H., and Gail, H. P. 2009. Abundances of the elements in the solar system. In Trümper, J. E. (Ed.), *LandoltBörnstein*, New Series, Vol. VI/4B. Berlin: Springer-Verlag, pp. 560–630.

Lugmair, G. W., and Shukolyukov, A. 1998. Early Solar System Timescales According to ^{53}Mn-^{53}Cr Systematics. *Geochimica et Cosmochimica Acta* 62: 2863–86.

Marty, B. 2012. The Origins and Concentrations of Water, Carbon, Nitrogen and Noble Gases on Earth. *Earth and Planetary Science Letters* 313: 56–66.

Mason, B. 1966. The Enstatite Chondrites. *Geochimica et Cosmochimica Acta* 30: 23–39.

McCoy, T. J. 1994. Partial Melting of the Acapulcoite-Lodranite Meteorite Parent Body. Doctoral dissertation. University of Hawai'i at Manoa.

McDonough, W. F. & 2003. Compositional model for the Earth's core. In Carlson, R. W. (Ed.), *Treatise on Geochemistry*: Amsterdam: Elsevier, pp. 547–68.

McKay, G., Le, L., Wagstaff, J., and Crozaz, G. 1994. Experimental Partitioning of Rare Earth Elements and Strontium: Constraints on Petrogenesis and Redox Conditions During Crystallization of Antarctic Angrite Lewis Cliff 86010. *Geochimica et Cosmochimica Acta* 58: 2911–9.

McKeegan, K. D., Chaussidon, M., and Robert, F. 2000. Incorporation of Short-Lived [10]Be in a Calcium-Aluminum-Rich Inclusion from the Allende Meteorite. *Science* 289: 1334–7.

Mezger, K., Maltese, A., and Vollstaedt, H. 2021. Accretion and Differentiation of Early Planetary Bodies as Recorded in the Composition of the Silicate Earth. *Icarus* 365: 114497.

Morgan, J. W., Higuchi, H., Takahashi, H., and Hertogen, J. 1978. A "Chondritic" Eucrite Parent Body: Inference from Trace Elements. *Geochimica et Cosmochimica Acta* 42: 27–38.

Mougel, B., Moynier, F., and Göpel, C. 2018. Chromium Isotopic Homogeneity Between the Moon, the Earth, and Enstatite Chondrites. *Earth and Planetary Science Letters* 481: 1–8.

Moynier, F., Dauphas, N., and Podosek, F. A. 2009. A Search for [70]Zn Anomalies in Meteorites. *The Astrophysical Journal Letters* 700:L92–5.

Nakagawa, Y., Sekiya, M., and Hayashi, C. 1986. Settling and Growth of Dust Particles in a Laminar Phase of a Low-Mass Solar Nebula. *Icarus* 67: 375–90.

Newsom, H. E. 1985. Molybdenum in Eucrites: Evidence for a Metal Core in the Eucrite Parent Body. *Journal of Geophysical Research: Solid Earth* 90: C613–7.

Newsom, H. E., and Drake, M. J. 1982. The Metal Content of the Eucrite Parent Body: Constraints from the Partitioning Behaviour of Tungsten. *Geochimica et Cosmochimica Acta* 46: 2483–9.

Newsom, H. E., and Drake, M. J. 1983. Experimental Investigation of the Partitioning of Phosphorus Between Metal and Silicate Phases: Implications for the Earth, Moon and Eucrite Parent Body. *Geochimica et Cosmochimica Acta* 47: 93–100.

Nittler, L. R., Alexander, C. M. O'D., Liu, N., and Wang, J. 2018. Extremely [54]Cr-and [50]Ti-Rich Presolar Oxide Grains in a Primitive Meteorite: Formation in Rare Types of Supernovae and Implications for the Astrophysical Context of Solar System Birth. *The Astrophysical Journal Letters* 856: L24.

Olsen, M. B., Wielandt, D., Schiller, M., Van Kooten, E. M., and Bizzarro, M. 2016. Magnesium and [54]Cr Isotope Compositions of Carbonaceous Chondrite Chondrules-Insights into Early Disk Processes. *Geochimica et Cosmochimica Acta* 191: 118–38.

Palme, H., and O'Neill, H. 2014. Cosmochemical Estimates of Mantle Composition. In Davis, A. M. (Ed.), *Planets, Asteroids, Comets and The Solar System*, Treatise on Geochemistry, Vol. 2. Amsterdam: Elsevier, pp. 1–39.

Pape, J., Mezger, K., Bouvier, A. S., and Baumgartner, L. P. 2019. Time and Duration of Chondrule Formation: Constraints from [26]Al-[26]Mg Ages of Individual Chondrules. *Geochimica et Cosmochimica Acta* 244: 416–36.

Patzer, A., and Schultz, L. 2001. Noble Gases in Enstatite Chondrites I: Exposure Ages, Pairing, and Weathering Effects. *Meteoritics & Planetary Science* 36: 947–61.

Petitat, M., Birck, J. L., Luu, T. H., and Gounelle, M. 2011. The Chromium Isotopic Composition of the Ungrouped Carbonaceous Chondrite Tagish Lake. *The Astrophysical Journal* 736: 23.

Qin, L., Alexander, C. M. O'D., Carlson, R. W., Horan, M. F., and Yokoyama, T. 2010. Contributors to Chromium Isotope Variation of Meteorites. *Geochimica et Cosmochimica Acta* 74: 1122–45.

Qin, L., Nittler, L. R., Alexander, C. M. O'D., Wang, J., Stadermann, F. J., and Carlson, R. W. 2011. Extreme [54]Cr-Rich Nano-Oxides in the CI Chondrite Orgueil—Implication for a Late Supernova Injection into the Solar System. *Geochimica et Cosmochimica Acta* 75: 629–44.

Ramdohr, P. 1963. The Opaque Minerals in Stony Meteorites. *Journal of Geophysical Research* 68: 2011–36.

Reedy, R. C., Arnold, J. R., and Lal, D. 1983. Cosmic-Ray Record in Solar System Matter. *Science* 219: 127–35.

Righter, K., and Drake, M. J. 1997. A Magma Ocean on Vesta: Core Formation and Petrogenesis of Eucrites and Diogenites. *Meteoritics & Planetary Science* 32: 929–44.

Rubie, D. C., Frost, D. J., Mann, U., Asahara, Y., Nimmo, F., Tsuno, K., and Palme, H. 2011. Heterogeneous Accretion, Composition and Core-Mantle Differentiation of the Earth. *Earth and Planetary Science Letters* 301: 31–42.

Rubie, D. C., Jacobson, S. A., Morbidelli, A., O'Brien, D. P., Young, E. D., de Vries, J., Nimmo, F., Palme, H., and Frost, D. J. 2015. Accretion and Differentiation of the Terrestrial Planets with Implications for the Compositions of Early-Formed Solar System Bodies and Accretion of Water. *Icarus* 248: 89–108.

Ruzicka, A., Snyder, G. A., and Taylor, L. A. 1997. Vesta as the Howardite, Eucrite and Diogenite Parent Body: Implications for the Size of a Core and for Large-Scale Differentiation. *Meteoritics & Planetary Science* 32: 825–40.

Sanloup, C., Jambon, A., and Gillet, P. 1999. A Simple Chondritic Model of Mars. *Physics of the Earth and Planetary Interiors* 112: 43–54.

Schiller, M., Bizzarro, M., and Fernandes, V. A. 2018. Isotopic Evolution of the Protoplanetary Disk and the Building Blocks of Earth and the Moon. *Nature* 555: 507–10.

Schönbächler, M., Carlson, R. W., Horan, M. F., Mock, T. D., and Hauri, E. H. 2010. Heterogeneous Accretion and the Moderately Volatile Element Budget of Earth. *Science* 328: 884–7.

Scott, E. R. D., and Krot, A. N. 2003. Chondrites and Their Components. *TrGeo* 1: 711.

Scott, E. R., Taylor, G. J., and Keil, K. 1993. Origin of Ureilite Meteorites and Implications for Planetary Accretion. *Geophysical Research Letters* 20: 415–8.

Shu, F. H., Shang, H., Glassgold, A. E., and Lee, T. 1997. X-Rays and Fluctuating X-Wings from Protostars. *Science* 277: 1475–9.

Shukolyukov, A., and Lugmair, G. W. 2006. Manganese–Chromium Isotope Systematics of Carbonaceous Chondrites. *Earth and Planetary Science Letters* 250: 200–13.

Stacey, F. D. 2005. High Pressure Equations of State and Planetary Interiors. *Reports on Progress in Physics* 68: 341–83.

Steenstra, E. S., Sitabi, A. B., Lin, Y. H., Rai, N., Knibbe, J. S., Berndt, J., Matveev, S., and van Westrenen, W. 2017. The Effect of Melt Composition on Metal-Silicate Partitioning of Siderophile Elements and Constraints on Core Formation in the Angrite Parent Body. *Geochimica et Cosmochimica Acta* 212: 62–83.

Sugiura, N., and Fujiya, W. 2014. Correlated Accretion Ages and ε[54]Cr of Meteorite Parent Bodies and the Evolution of the Solar Nebula. *Meteoritics & Planetary Science* 49: 772–87.

Taylor, G. J. 2013. The Bulk Composition of Mars. *Geochemistry* 73: 401–20.

Trinquier, A., Birck, J. L., and Allegre, C. J. 2007. Widespread [54]Cr Heterogeneity in the Inner Solar System. *The Astrophysical Journal* 655: 1179–85.

Trinquier, A., Birck, J. L., Allègre, C. J., Göpel, C., and Ulfbeck, D. 2008. [53]Mn–[53]Cr Systematics of the Early Solar System Revisited. *Geochimica et Cosmochimica Acta* 72: 5146–63.

Trinquier, A., Elliott, T., Ulfbeck, D., Coath, C., Krot, A. N., and Bizzaro, M. 2009. Origin of Nucleosynthetic Isotope Heterogeneity in the Solar Protoplanetary Disk. *Science* 324: 374–6.

Trønnes, R. G., Baron, M. A., Eigenmann, K. R., Guren, M. G., Heyn, B. H., Løken, A., and Mohn, C. E. 2019. Core Formation, Mantle Differentiation and Core-Mantle Interaction Within Earth and the Terrestrial Planets. *Tectonophysics* 760: 165–98.

Villeneuve, J., Chaussidon, M., and Libourel, G. 2009. Homogeneous Distribution of [26]Al in the Solar System from the Mg Isotopic Composition of Chondrules. *Science* 325: 985–8.

Vollstaedt, H., Mezger, K., and Alibert, Y. 2020. Carbonaceous Chondrites and the Condensation of Elements from the Solar Nebula. *The Astrophysical Journal* 897: 82.

Wadhwa, M., Zinner, E. K., and Crozaz, G. 1997. Manganese-Chromium Systematics in Sulfides of Unequilibrated Enstatite Chondrites. *Meteoritics & Planetary Science* 32: 281–92.

Wänke, H., and Dreibus, G. 1994. Chemistry and Accretion History of Mars. *Philosophical Transactions of the Royal Society of London, Series A: Physical and Engineering Sciences* 349: 285–93.

Warren, P. H. 2011. Stable-Isotopic Anomalies and the Accretionary Assemblage of the Earth and Mars: A Subordinate Role for Carbonaceous Chondrites. *Earth and Planetary Science Letters* 311: 93–100.

Wasserburg, G. J., Trippella, O., and Busso, M. 2015. Isotope Anomalies in the Fe-Group Elements in Meteorites and Connections to Nucleosynthesis in AGB Stars. *The Astrophysical Journal* 805: 7.

Wasson, J. T., and Kallemeyn, G. W. 1988. Compositions of Chondrites. *Philosophical Transactions of the Royal Society of London. Series A, Mathematical and Physical Sciences* 325: 535–44.

Weeks, K. S., and Sears, D. W. 1985. Chemical and Physical Studies of Type 3 chondrites—V: The Enstatite Chondrites. *Geochimica et Cosmochimica Acta* 49: 1525–36.

Weisberg, M. K., Prinz, M., Clayton, R. N., and Mayeda, T. K. 1993. The CR (Renazzo-Type) Carbonaceous Chondrite Group and its Implications. *Geochimica et Cosmochimica Acta* 57: 1567–86.

Weiss, B. P., Berdahl, J. S., Elkins-Tanton, L., Stanley, S., Lima, E. A., and Carporzen, L. 2008. Magnetism on the Angrite Parent Body and the Early Differentiation of Planetesimals. *Science* 322: 713–6.

Weyrauch, M., Horstmann, M., and Bischoff, A. 2018. Chemical Variations of Sulfides and Metal in Enstatite Chondrites—Introduction of a New Classification Scheme. *Meteoritics & Planetary Science* 53: 394–415.

Wilson, S. A. 1997. Data Compilation for USGS Reference Material BHVO-2, Hawaiian Basalt. US Geological Survey Open-File Report, 2–3.

Wood, B. J., Smythe, D. J., and Harrison, T. 2019. The Condensation Temperatures of the Elements: A Reappraisal. *American Mineralogist* 104: 844–56.

Woosley, S. E. 1997. Neutron-Rich Nucleosynthesis in Carbon Deflagration Supernovae. *The Astrophysical Journal* 476: 801–10.

Yamakawa, A., Yamashita, K., Makishima, A., and Nakamura, E. 2010. Chromium Isotope Systematics of Achondrites: Chronology and Isotopic Heterogeneity of the Inner Solar System Bodies. *The Astrophysical Journal* 720: 150–4.

Yoshizaki, T., and McDonough, W. F. 2020. The Composition of Mars. *Geochimica et Cosmochimica Acta* 273: 137–62.

Zhang, Y., Benoit, P. H., and Sears, D. W. 1995. The Classification and Complex Thermal History of the Enstatite Chondrites. *Journal of Geophysical Research: Planets* 100: 9417–38.

Zhu, K., Moynier, F., Wielandt, D., Larsen, K. K., Barrat, J. A., and Bizzarro, M. 2019. Timing and Origin of the Angrite Parent Body Inferred from Cr Isotopes. *The Astrophysical Journal Letters* 877: L13.

Zhu, K., Moynier, F., Schiller, M., and Bizzarro, M. 2020. Dating and Tracing the Origin of Enstatite Chondrite Chondrules with Cr Isotopes. *The Astrophysical Journal Letters* 894: L26.

Zhu, K., Sossi, P. A., Siebert, J., and Moynier, F. 2019. Tracking the Volatile and Magmatic History of Vesta from Chromium Stable Isotope Variations in Eucrite and Diogenite Meteorites. *Geochimica et Cosmochimica Acta* 266: 598–610.

Zipfel, J. & Palme, H. 1994. The Chemical Composition of Acapulco and Acapulcoites (abstract). 25th Lunar and Planetary Science Conference, p. 1563.

SUPPORTING INFORMATION

Additional supporting information may be found in the online version of this article.

Fig. S1. $\varepsilon^{54}Cr$ as a function of $\varepsilon^{53}Cr$ in physically separated metal-rich fractions (corrected for cosmogenic Cr using the equation given by Trinquier et al., 2007) from Sahara 97072 and Kota Kota. Both, corrected for cosmogenic Cr and uncorrected values are reported. The irradiation of Fe target produces cosmogenic Cr with $\varepsilon^{54}Cr/\varepsilon^{53}Cr = 3.6 \pm 0.2$ and irradiation of Ni produces cosmogenic Cr with $\varepsilon^{54}Cr/\varepsilon^{53}Cr = 1.4$. Slope of cosmogenic $\varepsilon^{54}Cr/\varepsilon^{53}Cr$ from lunar material = 2.6. The metal-rich fractions (excluding sulfide bearing metal (KK-M <80 μm) based on comparatively higher $\varepsilon^{53}Cr$ (from radiogenic ^{53}Mn), which causes deviation from the linear correlation) from both meteorites gives a slope in the $\varepsilon^{54}Cr$-$\varepsilon^{53}Cr$ correlation diagram 3.6 ± 0.4, which is similar to the irradiation of Fe targets. The slope of the $\varepsilon^{54}Cr$-$\varepsilon^{53}Cr$ correlation of metal fractions reduces to 2.9 ± 0.2 after adding the metal troilite spherules from Sahara 97072.

Fig. S2. $\varepsilon^{54}Cr$ versus $\varepsilon^{53}Cr$ in physically separated components of the EH3 chondrites Kota Kota and Sahara 97072 and data for chemical leachates of Kota Kota. The gray symbols are literature data for individual chondrule (Zhu et al., 2019, 2020) of Sahara 97096 (paired to Sahara 97072) Black crosses are literature data for whole rock samples from enstatite chondrites (Qin et al., 2010). Literature data for CC (dark red diamonds) and OC (dark green circles) group (Göpel et al., 2015; Qin et al., 2010; Trinquier et al., 2007, 2008) is shown for comparison. Different correlation lines (indicating variable slopes) for magnetic fractions and non-magnetic, slightly-magnetic and chondrule fractions and carbonaceous chondrite group (CC group) are shown for comparison.

Fig. S3. a) $\varepsilon^{54}Cr$ as a function of Fe/Cr variation in solar system objects. We also show data for individual groups of enstatite and ordinary chondrites (reference for literature data are mentioned in Table S2). The averages for OC and EC lie on the correlation line. However, data from individual OC and EC groups scatter around the correlation line because of variable Fe/Cr. This finding suggests that the fractionation of Fe/Cr between the groups may have occurred after the main episode of irradiation. b) $\varepsilon^{54}Cr$ as a function of Fe/Cr variation in physically separated components from Sahara 97072 and Kota Kota and of leachates from Kota Kota. c) $\varepsilon^{54}Cr$-Mn/Cr isochron diagram. If the proto-Earth is included, a broad correlation between $\varepsilon^{53}Cr$ and Mn/Cr is observed for inner solar system objects, reflecting the radiogenic ingrowth of ^{53}Cr from ^{53}Mn.

Fig. S4. $\varepsilon^{54}Cr$ as a function of Fe/Cr variation in physically separated components from Sahara 97072 and Kota Kota and average bulk rock value of EH chondrites from literature (Qin et al., 2010; Trinquier et al., 2007).

Table S1. $\varepsilon^{54}Cr$- $\varepsilon^{53}Cr$ values of individual standard measurements over the period of analyses.

Table S2. Ratios of Fe/Cr, Mn/Cr and Cr isotopes in the carbonaceous chondrites, enstatite chondrites, ordinary chondrites, Ureilite parent body (UPB), Acapulcoites, Angrites, Vesta, Earth, and Mars. Reported uncertainties on the Fe/Cr and Mn/Cr are 2 SD of the mean values from different analyses except Vesta and the Earth. Maximum uncertainties on the Fe/Cr and Mn/Cr for the Earth and Vesta are assumed to be 20% from the average values.

Table S3. $t = 300$ years, Solar fluence = 10,000 × current solar fluence. $\varepsilon^i X_{irr}$ = Irradiation produced isotope ratios of element X, ($\varepsilon^{53}Cr_{background} = -0.2$, $\varepsilon^{54}Cr_{background} = -1.5$).